# AUBURN UNIVERSITY

IR-05-02

# MECHANICALLY STABILIZED EARTH (MSE) REINFORCEMENT TENSILE STRENGTH FROM TESTS OF GEOTEXTILE REINFORCED SOIL

*Prepared by*

David J. Elton
Maria Aries Barrato Patawaran

JUNE 2005


GINN COLLEGE OF
ENGINEERING

**Highway Research Center**
Harbert Engineering Center
Auburn University, Alabama 36849-5337

www.eng.auburn.edu/research/centers/hrc.html

IR-05-02

# MECHANICALLY STABILIZED EARTH (MSE) REINFORCEMENT TENSILE STRENGTH FROM TESTS OF GEOTEXTILE REINFORCED SOIL

*Prepared by*

David J. Elton
Maria Aries Barrato Patawaran

JUNE 2005

# MECHANICALLY STABILIZED EARTH (MSE) REINFORCEMENT TENSILE STRENGTH FROM TESTS OF GEOTEXTILE REINFORCED SOIL

David J. Elton

Maria Aries Barrato Patawaran

## ABSTRACT

A MSE wall is inexpensive and is fairly easy to construct since it doesn't require skilled labor to lay out alternate layers of soil and reinforcement or perform compaction.

This technology can be utilized in bridge abutments by constructing shallow footings directly on top of the wall to support bridge girders, instead of using piles through the abutment.

By designing the abutment to carry the load, piles can be eliminated, generating savings in construction time and money. Moreover, since bridge resting on piles results in a bump at the end of the bridge due to uneven settlement between the abutment and the bridge, and MSE does not, since the bridge and the abutment settle at the same rate, the bump at the end of the bridge is eliminated.

Guidelines for calculating the required strength of geosynthetics to support bridges are presented.

# TABLE OF CONTENTS

# MECHANICALLY STABILIZED EARTH (MSE) REINFORCEMENT TENSILE STRENGTH FROM TESTS OF GEOTEXTILE REINFORCED SOIL

David J. Elton and Maria Aries Barrato Patawaran

## I. INTRODUCTION

Mechanically Stabilized Earth (MSE) is the general name for structures made of reinforced soil (Figure 1.1). Tensile reinforcement is placed between layers of soil to prevent it from failing. The reinforcement strengthens the soil, making it possible to build structures higher and stronger than soil-alone structures. The interaction between the reinforcement and the soil as a unit gives the mass greater strength than unreinforced soil. These structures serve as embankments, wingwalls, slope protection, steepened slopes and other places where a change in grade is required.

The earliest use of reinforced soil was to build walls such as the ziggurats in Iraq and the Great Wall of China. The ziggurat was reinforced with woven mats of reeds laid horizontally and with plaited ropes of the same material embedded in layers of sand and gravel while the Great Wall of China has tamarisk branches as reinforcement embedded in a mixture of clay and gravel. The concept of reinforced earth was introduced in the 1960s by Henri Vidal in France. The structure was composed of flat reinforcing metal strips embedded in the soil. In the 1970s the use of steel mesh or grid as reinforcement was introduced. The problem of corrosion of metal reinforcements and the emergence of geosynthetics later led to the latter's use as reinforcement.

The strength of a geosynthetic reinforced soil mass depends on the soil strength, the geosynthetic strength and the geosynthetic spacing. In order for reinforcement strength to be used, it must be mobilized. As the load is carried by the backfill between the reinforcements, the soil, which is much weaker than the geosynthetic, starts to slide against the reinforcement causing friction to develop, and mobilizing the reinforcement tensile strength. Reinforcement spaced too far apart leads to failure of the soil as if it were not reinforced at all. Thus, a close spacing is necessary to activate the reinforcement strength for the structure to be effective.

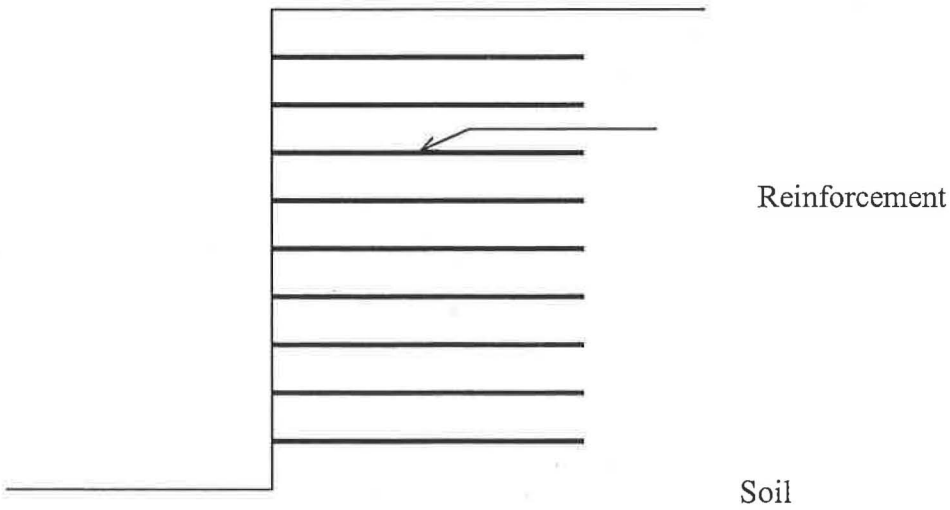


**Figure 1.1** Reinforced Soil

A MSE wall is inexpensive and is fairly easy to construct since it doesn't require skilled labor to lay out alternate layers of soil and reinforcement or perform compaction. This is a particularly attractive technology to a county engineer with a limited-skill workforce.

This technology can be utilized in bridge abutments by constructing spread foundation footings directly on top of the wall to support bridge girders. Bridge decks are normally supported by piles and are separate from the abutment. By designing the abutment to carry the load, piles can be eliminated, generating savings in construction time and money. A bridge resting on piles also results in a bump at the end of the bridge due to uneven settlement between the abutment and the bridge. Resting the bridge on the MSE allows the bridge and the abutment to act as a unit, giving uniform settlement and, therefore, eliminating that annoying bump at the end of the bridge.

Several piers and abutments have been built and tested and provided satisfactory results. Current design procedures, however, are considered very conservative. The mobilized strength of the reinforcement and its interaction with the soil during loading needs to be better defined to develop a design methodology that more closely resembles the actual conditions. Triaxial tests have been done on small samples in the laboratory. The reinforced samples showed increased strength and higher strain at failure than unreinforced ones. However, the spacing of the reinforcement is limited due to the small size of the samples. Therefore, large tests where reinforcement spacing is more realistic and similar to that in the field are needed.

## 1.1 Objectives

This project has these objectives:

1. Perform unconfined compression tests on large soil cylinders reinforced with geotextiles with more realistic reinforcement spacing than small triaxial samples.
2. Investigate the load carrying capacity of large geotextile reinforced soil samples.
3. Examine the soil and reinforcement behavior under loading.
4. Develop an equation to predict the tensile stress in the reinforcement.
5. Compare the developed equation with existing design methods.

## 1.2 Scope

The project covers:

1. Unconfined compression tests on 2.5 ft diameter, 5.0 ft high geosynthetic reinforced soil samples.
2. The use of poorly graded sand with less than 5% fines as backfill.
3. The use of spunbonded, needlepunched, nonwoven, polypropylene geotextiles of different mass/area as reinforcement.
4. Reinforcement spacing of 6 inches.
5. Analysis of the load carrying capacity of the reinforced soil samples.
6. Analysis of the strains in the reinforcement during loading with respect to their depth to height ratio
7. Development of the strain distribution factor based on reinforcement strains from the laboratory samples as well as from strains from walls found in literature.
8. Derivation of the equivalent lateral earth pressure coefficient.
9. Formulation of the equation to predict the tensile stresses in the reinforcement during loading.
10. Comparison of the proposed equation with NCMA (NCMA, 1996), Demo 82 (Elias and Christopher, 1996) and K Stiffness methods (Allen et al., 2003; Bathurst et al., 2003).

## 1.3 Limitations of Research

The research has the following limitations:

1. Only one type of backfill was used. The soil used was poorly graded sand with less than 5% fines.
2. A single reinforcement type was used. Spunbonded, needlepunched, nonwoven, polypropylene geotextiles with varying mass/area were used.
3. The vertical spacing of reinforcement was fixed at 6 inches.
4. The analysis was confined to developing a new equation for the tensile strength capacity of the reinforcement. No pullout analysis was performed.
5. The proposed equation was derived empirically.
6. The proposed equation was compared to the NCMA (NCMA, 1996), Demo 82 (Elias and Christopher, 1996), and K Stiffness methods (Allen et al., 2003; Bathurst et al., 2003).
7. Foundation conditions in the field may be different than that in the laboratory. The use of a steel base plate in the laboratory caused a foundation condition that was very stiff while the field foundation might not be stiff at all.

# II. LITERATURE REVIEW

A typical bridge deck normally rests on piles and separate from the abutment. When the abutment settles, the bridge deck, because it is on piles, doesn't settle at all. This causes differential settlement between the bridge and the abutment and results to a "bump" at the end of the bridge. A solution to this problem is to let the bridge deck sit on the abutment. When the abutment settles, the bridge, which is now part of the composite structure, settles with it. The uniform settlement between the bridge and the abutment results to a smooth transition and eliminates the "bump" at the end of the bridge.

A mechanically stabilized earth (MSE) abutment is an abutment where layers of reinforcement are sandwiched between layers of soil. This makes the soil stronger enabling it to carry the bridge deck on top of it. The strength of a reinforced soil mass depends on the reinforcement strength, the reinforcement spacing, and the soil strength. Initially, the applied load is carried by the soil until the soil starts to fail causing it to slide against the reinforcement. In order for the reinforcement strength to be utilized, it must be first set in motion. As slippage occurs between the soil and the reinforcement, friction is developed causing the reinforcement to stretch and mobilizing its strength. Reinforcement spaced too far apart leads to failure of the soil as if it were not reinforced at all. Thus, it is necessary to activate the reinforcement strength for the structure to be effective.

## 2.1 Reinforced Soil

### 2.1.1 History

The idea of reinforcing the soil to make it stronger thus making it possible to build taller structures is not new. Jones (1996) gives a comprehensive look into the history of reinforced soil. Agar-Quf or the ziggurat of Dur-Kurigatzu in Iraq and the Great Wall of China are reinforced soil structures that were built thousands of years ago and still exist today. The ziggurat was reinforced with woven mats of reed laid horizontally and with plaited ropes of reed embedded in layers of sand and gravel. The Great Wall of China has tamarisk branches as reinforcement embedded in a mixture of clay and gravel. Other ziggurats that were noted to have existed long ago were the structure at Ur (c. 2025 B.C.) and the Tower of Babel (c. 200 B.C.). The Romans used reeds as reinforcement in levees and used oak baulks in building wharfs. The Gauls used alternate layers of logs and soil to build forts.

Henri Vidal introduced the concept of reinforced earth in the 1960s in France (Jones, 1996; Vidal, 1969). The structure is composed of flat metal reinforcing strips embedded in the soil. The first facing was made from sheet metal which was later replaced by cruciform reinforcement concrete panels. The use of mesh or grid as reinforcement was introduced in the 1970s. The problem of corrosion and the emergence of geosynthetics later led to its use as reinforcement. The name mechanically stabilized earth (MSE) is now used to refer to reinforced soil structures.

### 2.1.2 Applications

The earliest use of reinforced soil was to build walls as in the ziggurats and the Great Wall of China as well as dykes in the Euphrates and Tigris (Jones, 1996). Presently, MSEs are used in landscaping walls, structural walls for change in grade, bridge abutments, stream channelization, waterfront structures, tunnel access walls, wing walls, and parking area support (NCMA, 1996). They are also used as temporary structures, dikes, dams, seawalls, and as bulk materials storage (Elias and Christopher, 1996). The use of MSEs as bridge abutments wherein the bridge deck is supported by the MSE instead of by piles is also possible (Abu-Hejleh, et al., 2000; Adams, 2000; Devin, et al., 2001; Powell, et al., 1999; Zornberg, et al., 2001)

### 2.1.3 Components

Reinforced soil has two main components: the backfill and the reinforcement. A facing is introduced if needed. Other components that are required are the foundation, drainage elements, and the connections between the facing and the reinforcement. Depending on the function of the reinforced soil being constructed, additional components may be needed.

#### 2.1.3.1 Backfill

Theoretically any type of soil can be used as backfill since the introduction of reinforcement would cause an increase in strength. However, prior to the mobilization of the reinforcement tensile strength, the soil alone carries the entire load. Soil contributes to the strength of the structure and how much load the soil can carry alone before the strength of the reinforcement is mobilized is important. Drainage characteristics and frost susceptibility are also essential in the selection of backfill. Thus, clean granular soils are preferred since they are stronger and drain better.

Select granular backfill material is required by the FHWA in the Demo 82 Manual (Elias and Christopher, 1996). It should conform to gradation requirements according to AASHTO T-27. Additional requirements are low plasticity, high internal friction angle, it should be free of shale or other soft, low-durability particles, should have a magnesium sulfate soundness loss of less than 30%, and it should meet the specified electrochemical criteria.

The NCMA Manual (NCMA, 1996) lists the advantages of granular backfill as ease in compaction, good drainage, stronger, and less susceptible to creep. As with Demo 82, NCMA prefers cohesionless material with less than 10% fines. However, soils with fines with low plasticity fines may be used as long as proper internal drainage is installed, the soil have low to moderate frost heave potential, the cohesion parameter is not considered in the stability analysis, and that the final design is checked by a qualified geotechnical engineer to ensure that any movement are within acceptable limits.

#### 2.1.3.2 Reinforcement

Different types of materials have been used as reinforcement. The reeds and branches used in ancient times have been replaced by metal and geosynthetics. Reinforcement can be in the form of strips, grids, and sheets.

##### 2.1.3.2.1Metal Reinforcement

Strip reinforcements are normally made from metals such as steel but they can also be made from aluminum, copper, polymers and glass fiber reinforced plastic (GRP). Those that are made from steel are stainless, galvanized, or coated, and can be plain or have protrusions (Jones, 1996). Wiremesh and geogrids are used. They have larger apertures.

#### 2.1.2.3.2 Geotextiles – woven and nonwoven

Woven geotextiles are made by weaving yarns using a weaving machine (Koerner, 1998). The warp direction is the direction the fabric is being made or the machine direction while the weft is the direction across the warp or the cross-machine direction.

Nonwoven geotextiles are further classified as heat-bonded, resin-bonded or needle-punched depending on the web-bonding process used (Koerner, 1998). For nonwoven geotextiles the cross-machine direction is typically stronger since the fabric is stretched in that direction during processing thus increasing its tensile strength.

## 2.2 Previous Triaxial Tests of Reinforced Soil

Numerous triaxial tests were carried out on sand reinforced with bronze discs (Long et al., 1983), geogrids (Futaki et al., 1990; Al-Omari et al., 1995) and geotextiles (Broms, 1977; Gray and Al-Refeai, 1986; Chandrasekaran et al., 1989; Atmazidis and Athanasopoulos, 1994; Bergado et al., 1995; Krishnasmawy and Isaac, 1995; Ashmawy and Bourdeau, 1998; Haeri et al., 2000). These tests were performed on small samples with diameters ranging from 36 mm (Gray and Al-Refeai, 1986) to a maximum of 200 mm (Chandrasekaran et al., 1989). Futaki et al. (1990) performed triaxial tests on huge samples with diameter of 1.6 m. The number of reinforcement layers used varied from a single layer in the middle up to numerous layers.

### 2.2.1 Reinforced soil strength

Triaxial test results show that addition of reinforcement causes increased peak strength, larger axial strain at failure, and reduced or limited post-peak loss of strength (Broms, 1977; Gray et al, 1982; Gray and Al-Refeai, 1986; Chandrasekaran et al., 1989; Ashmawy and Bourdeau, 1998; Haeri et al., 2000). The increase in strength was as much as four times that of unreinforced under drained conditions (Ashmawy and Bourdeau, 1998).

### 2.2.2 Effect of spacing

The increase in strength is influenced by the distance between the reinforcement as increasing the number of layers generally increases the load carrying capacity (Broms, 1977; Gray et al., 1982; Haeri et al., 2000). Several layers of low stiffness reinforcement are better than using few layers of high stiffness layers (Al-Omari et al., 1995).

### 2.2.3 Interface friction

The friction at the sand-geotextile interface is a big influence in the strength of the reinforced sample. Juran et al. (1988) attributed the strength of reinforced soil to the forces in the reinforcement and in cases where the reinforcement breaks, to the mobilized shearing resistance. The larger the interface friction the stronger the sample (Haeri et al., 2000).

### 2.2.4 Earth pressure coefficient

During triaxial loading, as the friction is mobilized between the soil and the reinforcement, the soil changes state from Ko to Ka and travels inward towards the center (Long et al., 1983). The section of the sample that remains at Ko condition at the core decreases as the spacing increases.

### 2.2.5 Normal stress

The normal stresses on the reinforced sample in compression are zero at the ends while maximum at the center (Chandrasekaran et al., 1989; Long et al., 1983). The samples tested by Long et al. (1983) showed that the edges fail first at strains as low as 0.4%. As the sample is loaded the edges fail first, reducing the normal stresses to zero, then moves towards the center where the normal stresses are maximum.

### 2.2.6 Angle of friction

Sample failure is two-fold (Figure 2.1): first there is slippage where the reinforcement and the soil starts to slip thereby mobilizing the interface friction, then failure as the reinforcement stretches and reaches its maximum tensile strength. Triaxial test results show that the failure

envelopes of reinforced samples, depending on sample size, are either bilinear or curved (Haeri et al., 2000). This confirms the results by Yang (1972) and by Gray et al. (1982) who found out that the break between the two kinds of failure occurs at a critical confining stress. The failure envelope at slippage is steeper than the soil's angle of internal friction but once the reinforcement starts to stretch the failure envelope tends to be parallel to the soil's angle of internal friction.

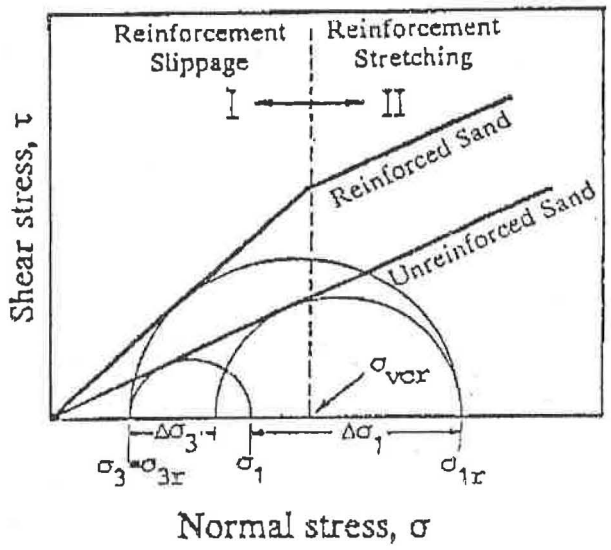


**Figure 2.1** Failure of Reinforced Soil (Atmatzidis and Athanasopoulos, 1994)

### 2.2.7 Need for bigger samples

Due to small sample size, however, the geotextiles can only be spaced as far apart as half the sample height. To get maximum spacing, only a single layer of reinforcement can be placed. To be able to put several layers of reinforcement in the sample, the reinforcements would have to be spaced closer to each other. This results to a spacing that is less than what is laid out in the field. Furthermore, Haeri et al. (2000) commented that smaller samples have higher peak strength and axial strain at failure. Thus, there is a need to build and test bigger samples. Larger samples would be more realistic and reinforcement spacing would be similar to that in the field.

## 2.3 MSE Bridge Abutments

There are existing bridges that are resting on MSE. The FHWA as part of its research has constructed a bridge pier (Adams, et al., 1999; Rekenthaler, 1997) and two bridge approaches (Adams, 2000) at the Turner-Fairbanks Highway Research Center in McLean, VA. The Colorado Department of Transportation (CDOT) built the Founders/Meadows Parkway bridge. The bridge abutment and two piers were built at the Havana site in Denver, CO in cooperation with the University of Colorado at Denver (Adams, et al., 1999; Wu, et al., 2001). Yenter Companies in Blackhawk, CO (Adams, et al., 1999) constructed two abutments reinforced with woven polypropylene geotextile to support a 36m span arch bridge.

The US Department of Agriculture, Forest Service (USFS) has built two MSE bridge abutments (Powell, et al., 1999) at Tongass National Forest in Alaska using high density polyethylene geogrid as reinforcement.

In Mammoth Lakes, CA two bridge abutments (Devin, et al., 2001) were constructed to replace the existing ones that were showing signs of deterioration. The abutments were reinforced with woven polypropylene geotextile.

Reinforced bridge abutments can also be found in other countries. Reinforced bridge abutments have been built in Australia (Boyd, 1988), Germany (Matichard et al., 1992), Hong Kong (Ng and Mak, 1988), Japan (Kasugai and Tateyama, 1992; Kumada et al., 1992), Jamaica (Barrett and Ruckman, 1996) and Spain (Boyd, 1988).

### 2.3.1 Load Carrying Capacity of MSE Bridge Abutments

The bridge pier (Figure 2.2) at the Turner-Fairbanks Highway Research Center in McLean, VA (Adams, et al., 1999; Ketchart and Wu, 2001) was successfully loaded to a pressure of 900 kPa (130.5 psi) with a maximum fabric strain of only 2.3%. The bridge pier was 5.4m (18 ft) high and reinforced with woven polypropylene geotextiles spaced 0.2m (8in) apart. The reinforcement has a wide-width tensile strength of 70 kN/m (400 lb/in).

The other two bridge approaches and abutments (Figure 2.3) built by FHWA (Adams, 2000) were also reinforced with woven polypropylene geotextile with tensile strengths ranging from 21 to 70 kN/m (120 to 400 lb/in) to a maximum height of 4.9m (16 ft). The abutments were loaded to 190 kPa (27.6 psi) with settlement observed at 10.5mm (0.40in). The abutments were designed to carry a load of 200 kPa (29.0 psi). For the load-bearing portion directly beneath the abutment seat, the reinforcement was closely spaced at 3 to 6in. The reinforcement spacing for the approaches was 0.3m (12in).

**Figure 2.2** The Bridge Pier at the Turner-Fairbanks Highway Research Center (http://www.tfhrc.gov/pubrds/winter97/p97wi43.htm)

**Figure 2.3** The Bridge Abutment at the Turner-Fairbanks Highway Research Center (http://www.tfhrc.gov/structur/gtr/main.htm)

The bridge abutment and two piers (Figure 2.4) built by Colorado Department of Transportation (CDOT) at the Havana site in Denver in cooperation with the University of Colorado at Denver (Adams, et al., 1999; Wu, et al., 2001) were reinforced with woven polypropylene geotextiles spaced 0.2 m (8in) apart. The outer pier and the abutment were both 7.6m (25 ft) high and were statically loaded up to 232 kPa (33.6 psi). The central pier was 7.3m (24 ft) high and was not loaded (Ketchart and Wu, 1997; Wu et al., 2001).

The Founders/Meadows Parkway bridge (Figure 2.5) was opened to traffic and monitoring results show the bridge performing well with negligible movements (Abu-Hejleh, et al., 2000; Abu-Hejleh, et al., 2001; Zornberg, et al., 2001). No bumps at the ends of the bridge were detected after 35 months in service (Abu-Hejleh, et al., 2003). It is reinforced with geogrids with long term wide-width design strengths of 6.8 to 27 kN/m (38.8 to 154 lb/in) spaced at 0.4m (16in). Its height varies, with a maximum height of 5.9m (19.4 ft).

The two abutments (Figure 2.6) constructed by Yenter Companies in Blackhawk, CO (Adams, et al., 1999; Ketchart and Wu, 2001) to support a 36m span arch bridge have heights varying from 1.5 to 7.5m (5 to 25 ft). The reinforcements were woven polypropylene geotextiles with wide-width tensile strength of 70 kN/m (400 lb/in) spaced 0.3m (12in) apart. The abutments were preloaded from 150 to 250 kPa (21.7 to 36.3 psi).

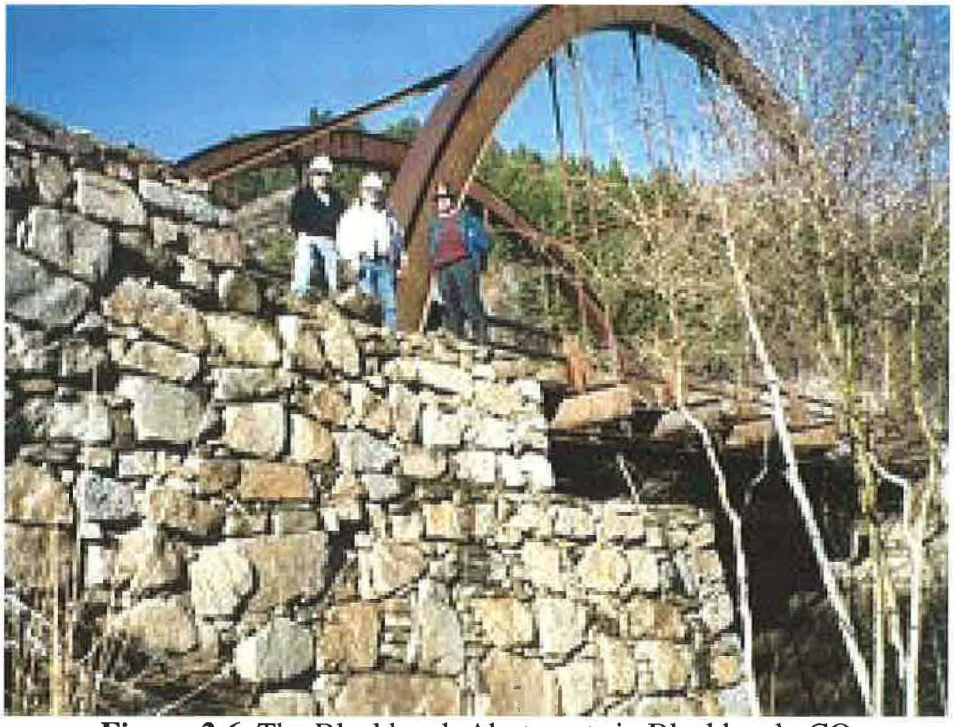

**Figure 2.6** The Blackhawk Abutments in Blackhawk, CO
(http://www.yenter.com/abutments.htm)

The two MSE bridge abutments (Powell, et al., 1999) built by the US Department of Agriculture, Forest Service (USFS) to support a 15.1m (49.5 ft) long bridge is 3.7m (12 ft) high. The combined dead and live load used for design was equivalent to an applied stress of 240 kPa (35 psi). High density polyethylene geogrids were used as reinforcement spaced 150mm (6in) near the top and 300mm (12in) near the base.

The two bridge abutments in Mammoth Lakes, CA (Devin, et al., 2001) has a maximum height of 6.5m (21.3 ft). In addition to the dead load, it was designed to carry a 14.4 kPa (2 psi) snow load, and was also designed to carry 0.5g seismic peak ground accelerations. The abutments were reinforced with woven polypropylene geotextile with tensile strengths ranging from 30.6 to 35 kN/m (174.8 to 200 lb/in) spaced at 0.15m (6in).

## 2.4 Design Guidelines

There are numerous guidelines that are currently used in the design of MSE. The most popular is the one released by the FHWA commonly known as DEMO-82 (Elias and Christopher, 1996). The National Concrete Masonry Association (NCMA) has its own guideline (NCMA, 1996) that is specifically for MSE that uses segmental units for its facing. In addition, Allen and Bathurst (Allen et al. 2003; Bathurst et al., 2003) empirically developed the K Stiffness Method through analysis of existing walls. The American Association of State Highway and Transportation Officials (AASHTO) has a section on MSE abutments as part of its LRFD Bridge Design Specifications (AASHTO, 1998).

### 2.4.1 External stability

External stability deals with the analysis of the soil mass brought about by its own weight and by the applied surcharge. Three factors are checked: sliding, overturning, and bearing capacity. Sliding is checked to ensure that the soil mass does not fail due to insufficient shear at its base. Overturning is checked to ensure that the soil mass does not rotate about its toe. The bearing capacity is checked to ensure that shear failure doesn't occur at its foundation. These analyses are well-known and well-documented in the literature.

### 2.4.2 Internal stability

Internal stability deals with the analysis of the stresses inside the structure. Tensile overstress is concerned with the tensile stresses in the reinforcement while pullout has to do with the slipping between the reinforcement and the backfill.

#### 2.4.2.1 Tensile overstress

Tensile stress in the reinforcement is affected by the soil type, depth of embedment, surcharge, and vertical spacing. The allowable tensile strength, Ta, of the geosynthetic reinforcement can be calculated as (Elias and Christopher, 1996):

$$T_a = \frac{T_{ult}}{RF_D \; RF_{ID} \; RF_{CR} \; FS}$$

where $T_{ult}$ is the ultimate or yield tensile strength from wide width tensile strength tests; FS is the overall factor of safety or load reduction factor to account for uncertainties in the geometry of the structure, fill properties, reinforcement properties, and externally applied loads; and $RF_D$, $RF_{ID}$, $RF_{CR}$ are the durability, installation damage, and creep reduction factors. Typical value for FS is 1.5. Typical ranges of reduction factors are 1.1 to 2.0 for durability, 1.05 to 3.0 for installation damage, and 1.5 to 5.0 for creep. The applied force in the reinforcement during loading should not exceed the allowable tensile strength.

#### 2.4.2.2 Pullout

Pullout is affected by the length of embedment of the reinforcement in the soil that is beyond the active failure surface. The resistance of the reinforcement against pullout is affected by the length of embedment and by the overburden pressure. NCMA (1996) recommends that the factor of safety against pullout be greater than or equal to 1.5. Demo 82 (Elias and Christopher, 1996) requires that the length of embedment be equal to the calculated embedment length or 1m whichever is greater.

## 2.5 Design Procedures

The equations used in the calculation of the tensile force in the reinforcement for the NCMA, Demo 82, and K Stiffness methods are discussed below.

### 2.5.1 National Concrete Masonry Association (NCMA) Method

The National Concrete Masonry Association (NCMA) published the Design Manual for Segmental Retaining Walls (SRW) to provide a standard analysis and design procedure for the industry. An SRW is constructed by dry-stacking segmental units which may be connected using concrete shear keys or other mechanical connectors. SRWs can either be conventional or reinforced. Conventional SRWs are those that rely on its self-weight and batter of the facing units to resist external forces. Reinforced SRWs are those that have an added resistance provided by geosynthetic reinforcement laid out in horizontal layers.

The tensile force in the reinforcement can be calculated as (NCMA, 1996):

$$F_{g(n)} = \left[\gamma_i D_n + q_l + q_d\right] K_a \cos\left(\delta_i - \omega\right) A_{c(n)}$$

where $\gamma_i$ is the backfill unit weight; $D_n$ is the depth to the midpoint of the contributory area, $A_{c(n)}$; $q_l$ and $q_d$ are the live and dead load surcharges; $K_a$ is the active earth pressure coefficient; $\delta_i$ is the interface friction angle between the soil and the reinforcement equal to $2\phi_i/3$; $\phi_i$ is the internal friction angle of the backfill; and $\omega$ is the wall inclination angle.

The contributory area of a reinforcement for any intermediate layer, $A_{c(n)}$, is given as the midpoint between two adjacent layers or between an adjacent layer and the top (topmost area, $A_{c(N)}$) or bottom (lowermost area, $A_{c(1)}$) of the wall and can be calculated as:

$$A_{c(1)} = (E_{(2)} + E_{(1)})/2$$

$$A_{c(n)} = (E_{(n+1)} - E_{(n-1)})/2$$

$$A_{c(N)} = H - [(E_{(n)} + E_{(n-1)})/2]$$

where $E_{(n)}$ is the reinforcement elevation measured from the heel of the lowermost unit.

The depth to the midpoint of the contributory area, $D_n$, of an intermediate layer for varying vertical spacing can be calculated as:

$$D_n = (H+h) - A_{c(1)} - A_{c(2)} - \ldots - A_{c(n-1)} - (A_{c(n)}/2)$$

For the uppermost layer it can be calculated as:

$$D_N = (A_{c(N)}/2)$$

For the lowermost layer it can be calculated as:

$$D_1 = (H + h) - (A_{c(1)}/2)$$

The active earth pressure coefficient, $K_a$, can be calculated using Coulomb's equation given as:

$$K_a = \frac{\cos^2(\phi_i + \omega)}{\cos^2\omega\cos(\omega - \delta_i)\left[1 + \sqrt{\frac{\sin(\phi_i + \delta_i)\sin(\phi_i - \beta)}{\cos(\omega - \delta_i)\cos(\omega + \beta)}}\right]^2}$$

For a vertical wall ($\omega = 0$) with a horizontal backslope ($\beta = 0$) and assuming that $\delta_i = 0$, $K_a$ can be calculated as:

$$K_a = \frac{1 - \sin\phi}{1 + \sin\phi}$$

### 2.5.2 DEMO-82

The Federal Highway Administration (FHWA) developed a manual for the design of Mechanically Stabilized Earth Walls (MSEW) and Reinforced Soil Slopes (RSS) for its Demonstration Project No. 82. The manual became the standard for the design of a number of MSEW and is more commonly called Demo 82.

The tensile force in the reinforcement can be calculated as (Elias and Christopher, 1996):

$$T_{max} = \sigma_H \cdot S_v$$

where $S_v$ is the vertical spacing between reinforcement layers and $\sigma_H$ is the horizontal stress acting on the reinforcement given as:

$$\sigma_H = K\sigma_v + \Delta\sigma_h$$

where $\Delta\sigma_h$ is the incremental horizontal stress due to a concentrated horizontal load. The ratio of the earth pressure coefficients, $K/K_a$, is a function of the reinforcement depth below the top of the wall (Figure 2.7). However, for geosynthetic reinforcements $K/K_a = 1$ regardless of depth. Therefore, $K = K_a$ for all layers of reinforcement. The active earth pressure coefficient can be calculated as:

$$K_a = \tan^2(45 - \phi/2)$$

The vertical stress, $\sigma_v$, can be calculated as:

$$\sigma_v = \gamma_r Z + q + \Delta\sigma_v$$

where $\gamma_r$ is the unit weight of the backfill, Z is the depth of soil at reinforcement layer, q is the surcharge load, and $\Delta\sigma_v$ is the incremental vertical stress due to a concentrated vertical load that can be calculated as shown in Figure 2.8 using a 2V:1H pyramidal distribution.

### 2.5.3 The K stiffness method

The Washington State Department of Transportation (WSDOT) with the Royal Military College in Kingston, Ontario, Canada, analyzed available load data from existing walls to develop

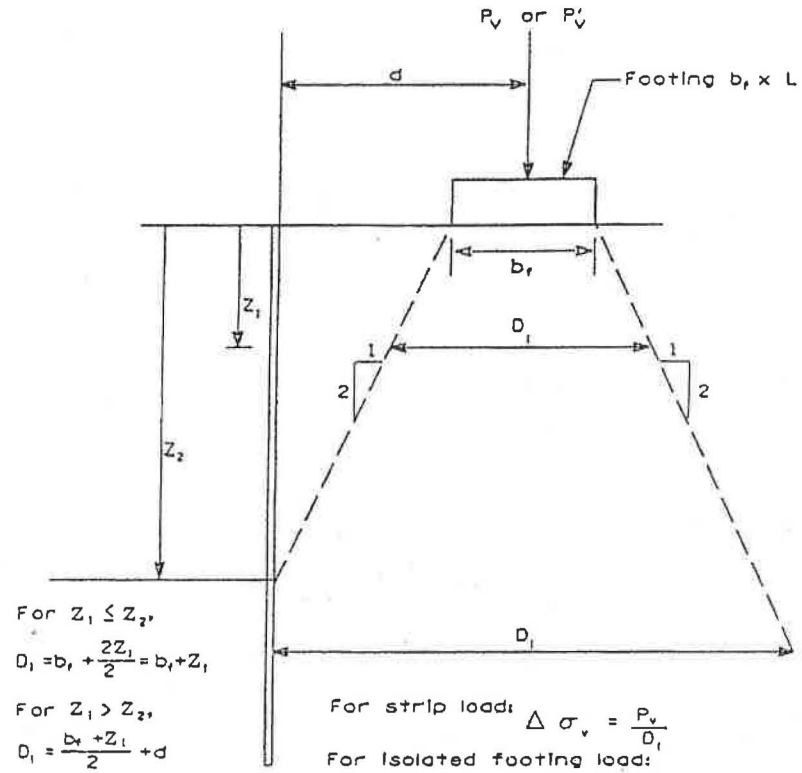


Where: $D_1$ = Effective width of applied load at any depth, calculated as shown above

$b_f$ = Width of applied load. For footings which are eccentrically loaded (e.g., bridge abutment footings), set $b_f$ equal to the equivalent footing width B' by reducing it by 2e', where e is the eccentricity of the footing load (i.e., $b_f - 2e'$).

L = Length of footing

$P_v$ = Load per linear meter (foot) of strip footing

$P_v'$ = Load on isolated rectangular footing or point load

$z_2$ = depth where effective width intersects back of wall face = 2d - p

Assume the increased vertical stress due to the surcharge load has no influence on stresses used to evaluate internal stability if the surcharge load is located behind the reinforced soil mass. For external stability, assume the surcharge has no influence if it is located outside th active zone behind the wall.

**Figure 2.8** Calculation of Vertical Load on an Abutment (Elias and Christopher, 1996)

The lateral earth pressure coefficient, $K_o$, is calculated using $1 - \sin \phi'$ where $\phi'$ is the backfill angle of internal friction. The facing stiffness factor, $\Phi_{fs}$, is recommended to be taken as equal to 0.5 for segmental concrete block and propped panel faced walls and 1.0 for all other types of wall facings. The local stiffness factor, $\Phi_{local}$, and the facing batter factor, $\Phi_{fb}$, are defined as:

$$\Phi_{local} = \left( \frac{S_{local}}{S_{global}} \right)^a$$

$$\Phi_{fb} = \left( \frac{K_{abh}}{K_{avh}} \right)^{d}$$

where a = 1.0 for geosynthetic walls, d = 0.5, and $K_{abh}$ and $K_{avh}$ are the horizontal components of the active earth pressure force accounting for wall face batter and the vertical wall, respectively. The local stiffness, $S_{local}$, considers the stiffness and reinforcement density at a given layer while the global stiffness, $S_{global}$, considers the stiffness of the entire wall section given below:

$$S_{local} = \frac{J}{S_v}$$

$$S_{global} = \frac{J_{ave}}{(H/n)} = \frac{\sum_{i=1}^{n} J_i}{H}$$

where J or $J_i$ is the modulus of an individual reinforcement layer, $J_{ave}$ is the average modulus of all the reinforcement layers and n is the number of reinforcements within the entire wall section.

## 2.6 Design Parameters

The NCMA, Demo 82 and the K Stiffness Methods equations to calculate the tensile stresses in the reinforcement may look different from each other but they actually are similar. They have parameters in their equations that are unique to each method but they also have some common factors. The vertical stress, the earth pressure coefficient, and the vertical spacing can all be found in each of the equations.

### 2.6.1 Vertical stress

The total vertical stress in the NCMA, Demo 82 and K Stiffness Methods takes various forms. In the NCMA and Demo 82 methods, it is taken as the backfill stress plus any other vertical surcharge. The backfill stress is calculated as the product of the backfill unit weight and the depth of the soil at the reinforcement layer. The vertical stress, $\sigma_v$, on the reinforcement is calculated as:

$$\sigma_v = \gamma_i D_n + q_l + q_d$$

for the NCMA method (NCMA, 1996) where $\gamma_i$ is the backfill unit weight, $D_n$ is the depth to the midpoint of the contributory area and $q_l$ and $q_d$ are the live and dead load surcharges.

The Demo 82 method (Elias and Christopher, 1996) calculates the vertical stress, $\sigma_v$, on the reinforcement as:

$$\sigma_v = \gamma_r Z + q + \Delta\sigma_v$$

where $\gamma_r$ is the unit weight of the backfill, Z is the depth of soil at reinforcement layer, q is the surcharge load, and $\Delta\sigma_v$ is the incremental vertical stress due to a concentrated vertical load discussed earlier.

The K Stiffness method calculates the vertical stress as the sum of the embankment height and the surcharge height multiplied by the unit weight of the backfill. The vertical stress, $\sigma_v$, on the reinforcement is calculated as (Bathurst et al., 2003; Allen et al., 2003):

$$\sigma_v = \gamma (H + S)$$

where $\gamma$ is the backfill unit weight, H is the height of the wall, S is the average height of the soil surcharge.

### 2.6.2 Earth pressure coefficient

The actual state of stress of the sample during loading is still unknown. From triaxial tests of reinforced soil, Long et al. (1983) discovered that during loading, the soil changes state from

$K_o$ to $K_a$ and travels inward towards the center as the friction is mobilized between the soil and the reinforcement. The NCMA and Demo 82 methods use the active earth pressure coefficient while the K stiffness method uses the at-rest earth pressure coefficient in their equation.

The NCMA method (NCMA, 1996) uses the active earth pressure coefficient, $K_a$, in the tensile stress equation calculated using Coulomb's equation given as:

$$K_a = \frac{\cos^2(\phi_i + \omega)}{\cos^2\omega\cos(\omega - \delta_i)\left[1 + \sqrt{\frac{\sin(\phi_i + \delta_i)\sin(\phi_i - \beta)}{\cos(\omega - \delta_i)\cos(\omega + \beta)}}\right]^2}$$

where $\phi_i$ is the peak internal friction angle of the backfill, $\delta_i$ is the interface friction angle between the backfill and the reinforcement, $\omega$ is the wall facing batter, and $\beta$ is the backslope angle with respect to the horizontal measured in a counter-clockwise direction. For a vertical wall ($\omega = 0$) with a horizontal backslope ($\beta = 0$, $\delta = 0$) $K_a$ can be calculated as:

$$K_a = \frac{1 - \sin\phi}{1 + \sin\phi}$$

The earth pressure coefficient, K, used in the Demo 82 method (Elias and Christopher, 1996), is dependent on the active earth pressure coefficient. The ratio of the earth pressure coefficients, $K/K_a$, is a function of the reinforcement depth below the top of the wall and is given in Figure 2.7. The ratio $K/K_a$ is equal to unity regardless of depth for geosynthetic reinforcements. Therefore, $K = K_a$ for all layers of geosynthetic reinforcement. The active earth pressure coefficient can be calculated using Rankine's equation as:

$$K_a = \tan^2(45 - \phi/2)$$

The K Stiffness method (Bathurst et al., 2003; Allen et al., 2003), uses the at-rest earth pressure coefficient, $K_o$, calculated as:

$$K_o = 1 - \sin\phi'$$

where $\phi'$ is the angle of internal friction of the backfill.

### 2.6.3 Vertical spacing

The triaxial tests on small reinforced samples showed that the spacing of the reinforcement influences the increase in strength of the reinforced sample. An increase in the number of layers or a decrease in the reinforcement spacing lead to an increase in the sample strength (Broms, 1977; Gray et al., 1982; Haeri et al., 2000).

Numerical models by Vulova and Leshchinsky (2003) showed that reinforcement spacing is a critical factor in the failure of a reinforced wall and controls the mode of failure shifting from external or deep-seated to compound and finally to connection failure as the spacing is increased. A critical spacing of 0.4m (15.75 in) was determined with results showing that reinforcement spacing greater than 0.4m (15.75 in) would result to internal instability within the wall. Walls with reinforcement spacing equal to or greater than 0.6m (23.60 in) did not move as a coherent mass and experienced large deformations leading to failure at the connections.

The NCMA, Demo 82 and the K stiffness methods consider the effect of reinforcement spacing by using the parameter $A_{c(n)}$ for NCMA (NCMA, 1996), and the parameter $S_v$ for Demo 82 (Elias and Christopher, 1996) and K stiffness (Bathurst et al., 2003; Allen et al., 2003) methods in their equations.

### 2.6.4 Other parameters

The NCMA, Demo 82 and K stiffness methods have common factors between them but within each equation are parameters that are unique to each method.

The NCMA method (NCMA, 1996) has the factor cos ($\delta_i$ - $\omega$) where $\delta_i$ is the interface friction angle between the soil and the reinforcement equal to $2\phi_i/3$; $\phi_i$ is the internal friction angle of the backfill; and $\omega$ is the wall inclination angle.

The Demo 82 method (Elias and Christopher, 1996) accounts for the incremental horizontal stress, $\Delta\sigma_h$, due to a concentrated horizontal load.

The K Stiffness method (Bathurst et al., 2003; Allen et al., 2003) has the factors $D_{t\ max}$, $\Phi_{local}$, $\Phi_{fb}$, $\Phi_{fs}$, $S_{global}$ and $p_a$. The parameter $D_{t\ max}$ is the distribution factor (Allen and Bathurst, 2001); $\Phi_{local}$, $\Phi_{fb}$, and $\Phi_{fs}$ are the local stiffness, facing batter, and facing stiffness factors; $S_{global}$ is the global reinforcement stiffness; and $p_a$ is the atmospheric pressure constant.

# III. LABORATORY TESTING

Large, cylindrical, reinforced soil samples were tested in unconfined compression. The samples were 2.5 ft in diameter and 5.0 ft high. The backfill used was poorly graded sand reinforced with nonwoven geotextiles of varying strengths. The vertical reinforcement spacing was 6 in and 12 in.

## 3.1 Materials

The most important components of a mechanically stabilized earth (MSE) wall or abutment are the backfill and the reinforcement. They are the parts that contribute to the strength of the structure.

### 3.1.1 Backfill

The backfill soil used in the research was classified as poorly graded sand (Unified Soil Classification System symbol SP) with less than 5% fines. Grain size analyses were performed on the backfill soil before and after the tests (Table 3.1). The grain size distribution curves are presented in Figure 3.1 showing no significant difference between the two.

Compaction tests (Modified Proctor, ASTM D1557) done on the soil showed an optimum moisture content of about 9.3% and a maximum dry unit weight of about 121 pcf. The results of the compaction test are given in Table 3.2 and the Proctor curve is presented in Figure3.2.

**Table 3.1** Results of Grain Size Analyses Before and After the Compression Test

| Sieve No | Diameter (mm) | % Passing Before | %Passing After |
|---|---|---|---|
| 1/2 in | 12.5 | 98.35 | 97.85 |
| 0.375 in | 9.5 | 97.03 | 96.85 |
| 4 | 4.75 | 94.44 | 94.08 |
| 10 | 2.0 | 87.62 | 87.73 |
| 16 | 1.18 | 80.35 | |
| 20 | 0.84 | | 66.79 |
| 40 | 0.425 | 25.87 | 39.09 |
| 60 | 0.25 | 13.37 | 20.02 |
| 80 | 0.18 | 7.76 | 12.71 |
| 100 | 0.15 | 5.47 | 7.89 |
| 200 | 0.075 | 1.03 | 2.05 |

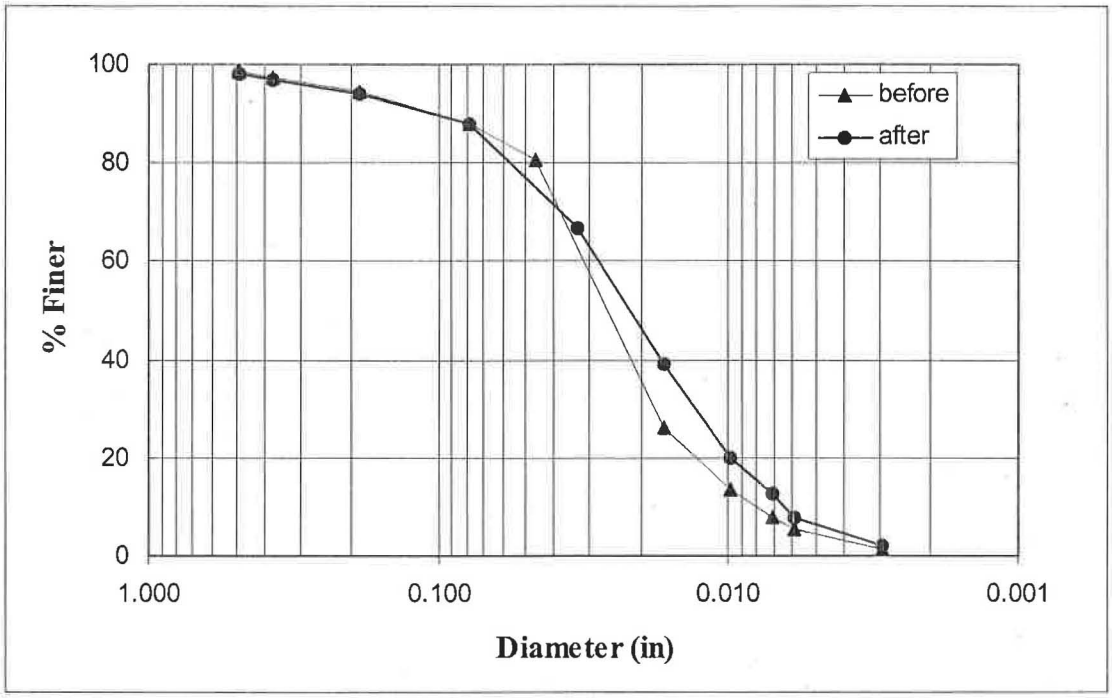


**Figure 3.1** Backfill Grain Size Distribution Before and After the Compression Test

**Table 3.2** Proctor Compaction Test Results on Backfill

| Water Content (%) | Dry Unit Weight (pcf) |
|---|---|
| 4.43 | 115.37 |
| 6.05 | 117.41 |
| 7.70 | 119.38 |
| 9.45 | 121.03 |
| 11.78 | 117.85 |
| 13.26 | 117.47 |

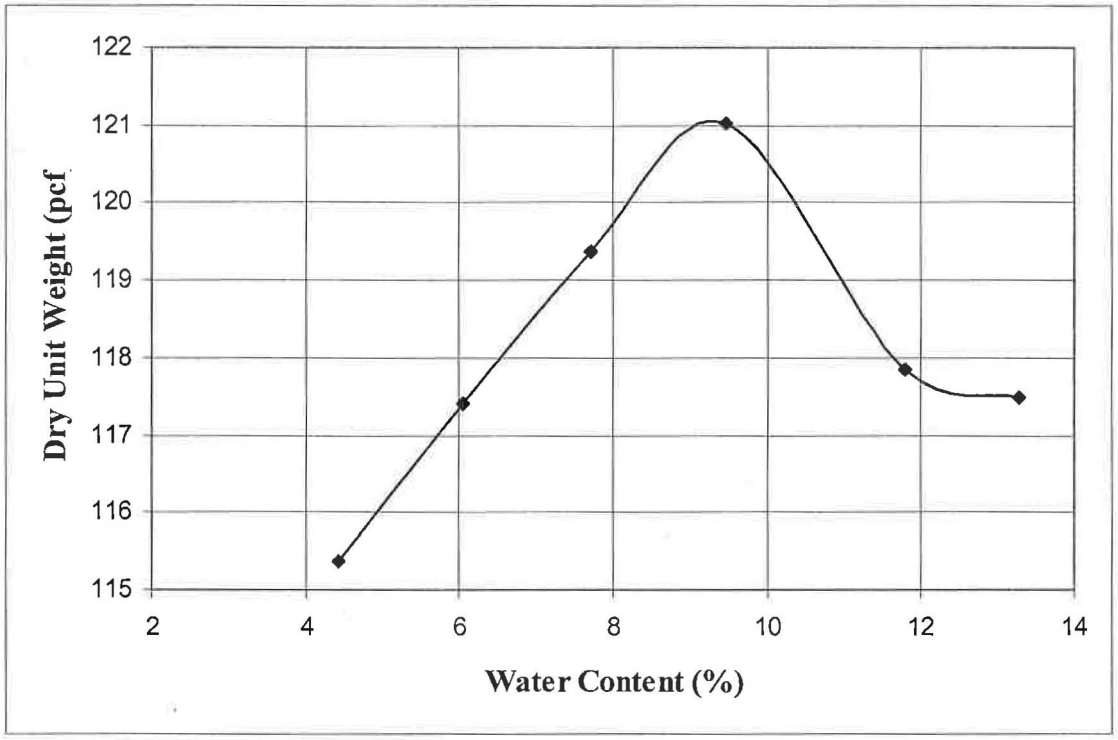


**Figure 3.2** Backfill Compaction Curve

Direct shear test (ASTM D3080) results on the compacted soil show an angle of internal friction of 40° and a cohesion of about 4 psi. The results of the direct shear test are given in Table 3.3 and plotted in Figure 3.3.

**Table 3.3** Direct Shear Test Results on the Backfill

| Normal Stress (psi) | Shear Stress (psi) |
|---|---|
| 2.15 | 5.89 |
| 3.99 | 7.41 |
| 5.82 | 9.03 |

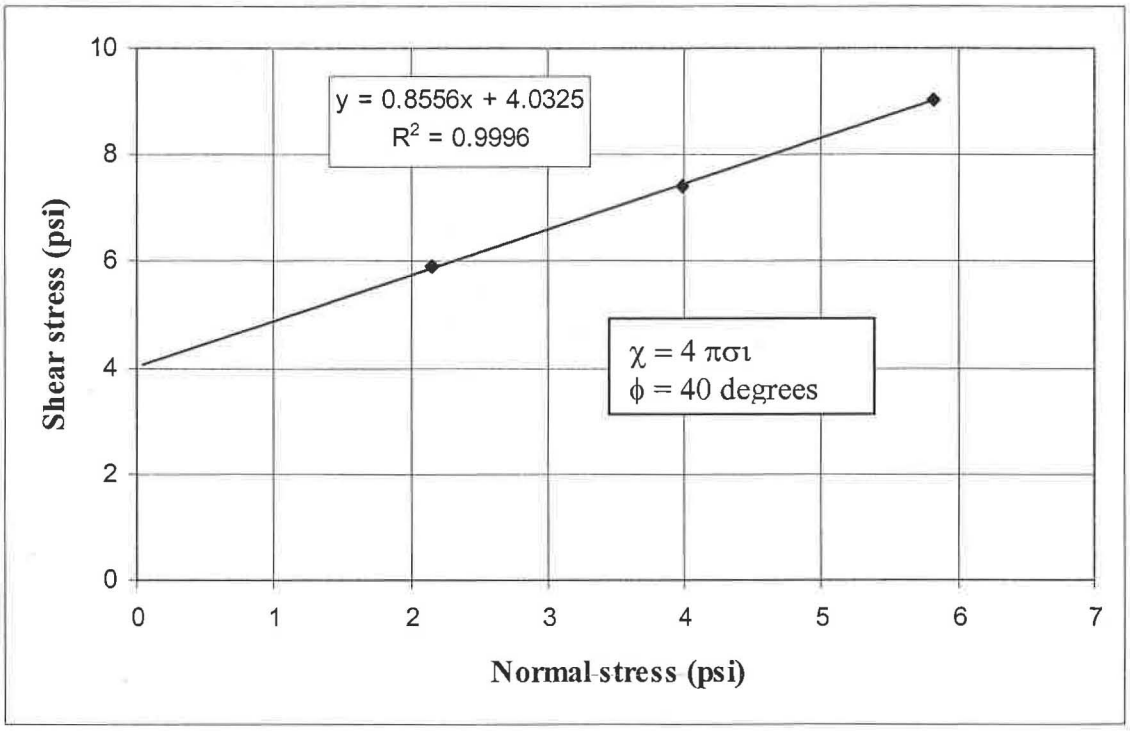


**Figure 3.3** Direct Shear Test Results of Backfill

### 3.1.1 Reinforcement

The study used spunbonded, needlepunched, nonwoven, polypropylene geotextiles named TG500, TG600, TG700, TG800, TG1000 and TG028 of different masses/area. The geotextiles were provided by Evergreen Technologies, Inc. Table 3.4 gives the physical and mechanical properties of the geotextiles as provided by the manufacturer, except for the wide-width test (ASTM D4595) results in the machine and cross-machine directions, which were performed in the Auburn Textile Engineering laboratory.

**Table 3.4** Geotextile Properties

| Property | Test Method | TG 500 | TG 600 | TG 700 | TG 800 | TG 1000 | TG 028 |
|---|---|---|---|---|---|---|---|
| **Physical** | | | | | | | |
| Mass/Area (oz/yd$^2$) | ASTM D 5261 | 4.0 | 6.0 | 8.0 | 12.0 | 16 | 28 |
| Thickness (mils) | ASTM D 5199 | 45 | 65 | 85 | 120 | 155 | 238 |
| **Mechanical** | | | | | | | |
| Grab Strength (lbf) | ASTM D 4632 | 120 | 160 | 215 | 350 | 400 | 520 |
| Grab Elongation (%) | ASTM D 4632 | 50 | 50 | 50 | 50 | 50 | 50 |
| Tear Strength (lbf) | ASTM D 4533 | 45 | 65 | 85 | 120 | 135 | 220 |
| Mullen Burst (psi) | ASTM D 3786 | 215 | 285 | 375 | 575 | 675 | 720 |

| | | | | | | | |
|---|---|---|---|---|---|---|---|
| Puncture Resistance (lbf) | ASTM D 4833 | 60 | 80 | 100 | 145 | 170 | 200 |
| U.V. Resistance (%) | ASTM G 53 | 70 | 70 | 70 | 70 | 70 | 70 |
| Wide-width MD* (lb/in) | ASTM D 4595 | 51 | 80 | 83 | 106 | 115 | 142 |
| Wide-width XMD* (lb/in) | ASTM D 4595 | 82 | 110 | 113 | 116 | 131 | 124 |
| Elongation at Break MD* (%) | | 135 | 135 | 161 | 123 | 132 | 50 |
| Elongation at Break XMD* (%) | | 40 | 45 | 57 | 33 | 45 | 81 |
| Tangent Modulus MD* (lb/in) | | 75 | 110 | 132 | 214 | 238 | 602 |
| Tangent Modulus XMD* (lb/in) | | 365 | 462 | 450 | 646 | 539 | 454 |

*MD = Machine Direction; XMD = Cross-machine Direction
1 oz/yd$^2$ = 33.91 g/m$^2$; 1 mil = 0.0254 mm; 1 lbf = 4.45 N; 1 psi = 6.89 kPa; 1 lb/in = 0.1752 kN/m

The mass per unit area of the reinforcements varied from 4 oz/yd$^2$ for TG500 to 28 oz/yd$^2$ for TG028. The thinnest reinforcement was TG500 (45 mils) while the thickest reinforcement was TG028 (238 mils).

The wide-width tensile strengths in the weaker direction, normally in the machine direction except for TG028, were taken as the reinforcement tensile strength. The range of tensile strengths varied from 51 lb/in for TG500 to 124 lb/in for TG028. The wide-width tensile strengths of TG600, TG700, TG800 and TG1000 are 80 lb/in, 83 lb/in, 106 lb/in and 115 lb/in, respectively.

### 3.1.2 Other components of MSE

Other components of an actual MSE wall or abutment are the optional facing, the drainage components and the leveling pad. These are not discussed here since they are beyond the scope of the project.

## 3.2 Testing Procedure

### 3.2.1 Sample preparation

#### 3.2.1.1 Mold

The test specimens were constructed inside 2.5-ft diameter, 1/4-inch thick Kirkpatrick cylindrical cardboard tubes, normally used in concrete pours.

#### 3.2.1.2 Soil preparation

The backfill was stored and mixed to optimum moisture content in large, steel boxes. The boxes were weighted before and after soil placement to determine the weight of the soil in the mold.

#### 3.2.1.4 Soil placement – Stage I

The prepared soil was shoveled into the mold and each 6-inch lift was compacted to 95% of the modified Proctor density (ASTM D1557) using a hand-held pneumatic compactor (Figure 3.4). The top of the layer was leveled using a steel plate and a nuclear density gauge (Figure 3.5) verified the compaction density.

#### 3.2.1.5 Geotextile preparation and placement

The geotextiles were cut from the roll using a 2.5 ft diameter plywood template and a sharp box cutter. The cut reinforcement was then laid out carefully on the surface of the

compacted soil to eliminate wrinkles. All reinforcements were oriented in the same, machine, direction at each level. The reinforcements were initially placed at 12-inch spacing for TG500. The vertical spacing was later reduced to 6-inch spacing, which was used for all the reinforcements.

**3.2.1.6 Soil placement – Stage II**

The mold restraint was removed after compaction of the fifth lift, and the top half of the mold was placed onto the bottom half. The mold restraint was then put back to hold the now 5.5-ft high mold in place. The extra half a foot of mold at the top was provided to hold the loose soil prior to compaction. The finished compacted specimen was slowly moved into place, centered under the loading ram, by lifting the sample at the base plate by the forklift (Figure 3.6). The straps and the mold were then removed (Figure 3.7).

**Figure 3.4** Compaction of Sample Using a Pneumatic Compactor

**Figure 3.5** Nuclear Density Gauge Checks the Density

**Figure 3.6** The Sample was Placed Under the Loading Ram by a Forklift.

#### 3.2.1.3 Compression testing

The specimen was loaded in unconfined compression by lowering the loading plate. During loading, the vertical displacement and the applied load were monitored through the data acquisition system. The test was stopped once the load reading started to decrease dramatically, the point where the sample was considered to have failed.

### 3.2.2 Instrumentation

#### 3.2.2.1 Load

A load cell and three displacement transducers provided the data for strength and deformation parameters needed for analysis. A load cell was attached to the hydraulic ram (Figure 3.8).

#### 3.2.2.2 Vertical deflection

To measure the vertical deformation of the sample during loading, three transducers were attached to the top of the steel loading plate (Figure 3.9). The transducers were mounted on a steel frame and were arranged in a triangle, equidistant to each other. The frame was positioned on top of the loading plate and centered on the sample. The transducers were connected to the loading plate by attaching the cables to the magnetic hooks placed on top of the plate directly below the transducers.

#### 3.2.2.3 Lateral deflection

Lateral displacement measurements were made with linear transducers attached to a frame next to the specimen (Figure 3.11). Fabric pins, made of 3/16-inch steel wire with a 1-1/2 inch washer welded at the ends (Figure 3.10), were cut to 4-inch lengths and hammered into the sample. The pins served as the contact point for the lateral transducers. The pins were placed where the geotextiles were: at 1.5 ft, 2.5 ft, and 3.5 ft from the base plate at one side; and at 2.0 ft, 3.0 ft, and 4 ft from the base plate at the opposite side.

The transducer shafts were extended to their full length and their ends positioned next to the washer of the fabric pins that were hammered into the sample. The extended transducer shortens as it was pushed back into the shaft as the sample bulged during loading.

#### 3.2.2.4 Data acquisition

An automated data acquisition system, monitored and recorded data from the load cell and the vertical and lateral displacement transducers every second.


**Figure 3.7** Reinforced Cylinder Prior to Testing

**Figure 3.8** The 300-kip Compression Loadcell

**Figure 3.9** Cable Extension Displacement Transducers


**Figure 3.10** Fabric Pin with Washer

**Table 4.1** Unconfined Compression Test Results

| Reinforcement | Reinf. Spacing (in) | Reinforcement Modulus (lb/in) | Strain Rate (%/min) | Peak Strength (ksf) | Vertical Strain at Peak (%) |
|---|---|---|---|---|---|
| TG500 | 12 | 75 | 9.6 | 2.7 | 1.7 |
| TG500 | 6 | 75 | 7.8 | 4.8 | 3.1 |
| TG600 | 6 | 110 | 7.3 | 6.4 | 3.9 |
| TG700 | 6 | 132 | 6.5 | 6.1 | 4.5 |
| TG800 | 6 | 214 | 5.8 | 8.4 | 4.7 |
| TG1000 | 6 | 238 | 6.0 | 8.3 | 7.7 |
| TG028 | 6 | 454 | 6.9 | 9.6 | 8.5 |

Consider a typical single-span, short (about 50 ft ) concrete bridge with two-12 ft lanes weighing about 300 kips. Assuming two 75-kip trucks on one end of the bridge near the abutment, the load bearing on a 5 ft x 24 ft bridge seat would produce a stress of about 2.5 ksf. The strength of the laboratory sample reinforced with TG500 at 6-inch spacing, 4.8 ksf, exceeded this value. This strongly suggests that reinforced soil moderately reinforced with a 50 lb/in wide-width tensile strength geotextile spaced at 6 inches can support a modest single span bridge.

**4.2 Sample Deformation**

The rate of deformation of each specimen was dependent on the strength of the reinforcement in it. The deformation rate of each sample was determined by plotting the vertical displacement with time as shown in Figure 4.2. Each specimen showed a linear rate of deformation during loading with the weaker reinforcement exhibiting a faster rate of deformation. The sample reinforced with TG500 spaced at 12 inches displayed the fastest rate of deformation. Visual inspection of the reinforcement after the test showed no damage to the geotextiles. It is possible that due to very large spacing between the reinforcements, the entire load was absorbed by the soil during compression. Thus, the tensile strength of the reinforcement was never mobilized and the reinforcement did not contribute to the strength at all. For this reinforcement spacing, the sample failed due to soil failure alone. Therefore, a 12-inch spacing was considered too far apart for the reinforcement to contribute to the strength and further tests were done at 6-inch reinforcement spacing.

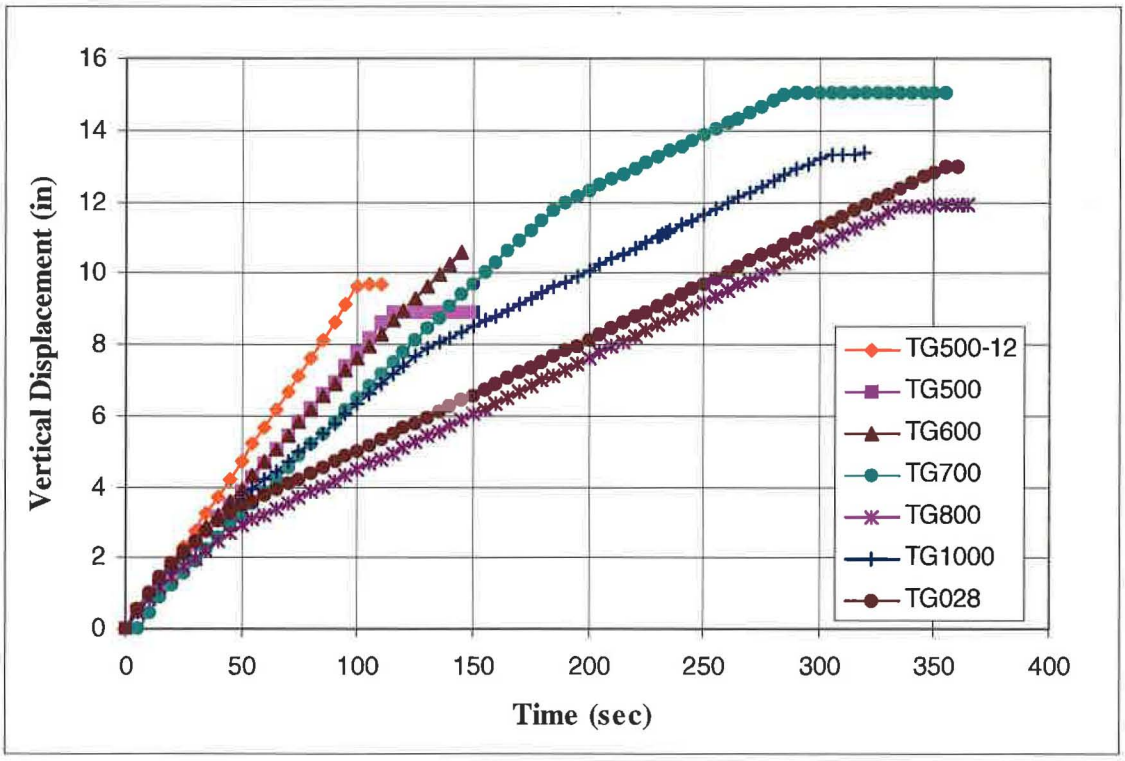


**Figure 4.2** Plot of Vertical Displacement with Time

### 4.3 Stresses in the Reinforcement

The reinforcements used in this experiment were nonwoven geotextiles that have different tensile strengths in the machine and cross-machine directions with the latter, generally, having higher strength compared to the former. As the tensile strength of the reinforcement was mobilized, the geotextile stretched, causing tearing in some layers.

The geotextile tears were linear and were perpendicular to the machine direction. This was consistent in all torn geotextiles, and was expected, since the machine direction is the weaker direction.

Figure 4.3 shows the tear locations for TG500, TG600, TG700 and TG028. Reinforcement TG500 had 6 layers of torn geotextiles while reinforcements TG600 and TG700 both had two torn layers. Reinforcement TG800 only had a single torn layer, near the middle layer. No tears were observed for reinforcements TG1000 and TG028. The pattern of tears suggests that the first layer to tear was the fourth layer from the top, approximately the middle of the specimen. This can be an indication that the first layers to be mobilized and reach their tensile strength were the middle layers. This also suggests that more lateral strain occurred in the middle part of the sample, than at the ends.

### 4.4 Strains in the Reinforcement

The initial diameter of the reinforcement was 30 inches. As the sample was taken apart layer by layer after testing, the final diameter of the reinforcement was measured to determine the permanent amount of strain.

To compare how much a layer stretches with respect to the other layers, the individual strain in each layer was normalized by the maximum strain among all the layers in the sample. The plot of the normalized strain along the machine direction against its depth normalized by the total height is given in Figure 4.4.

The plot shows that all the points can be bounded by three lines. The normalized strains are unity for z/H ranging from 0.20 to 0.80 where z is the depth of the reinforcement measured from the top and H is the height of the sample or wall. At z/H less than 0.20 and greater than 0.80 the normalized strains are bounded by lines that extend from 1.0 and decreasing linearly to zero.

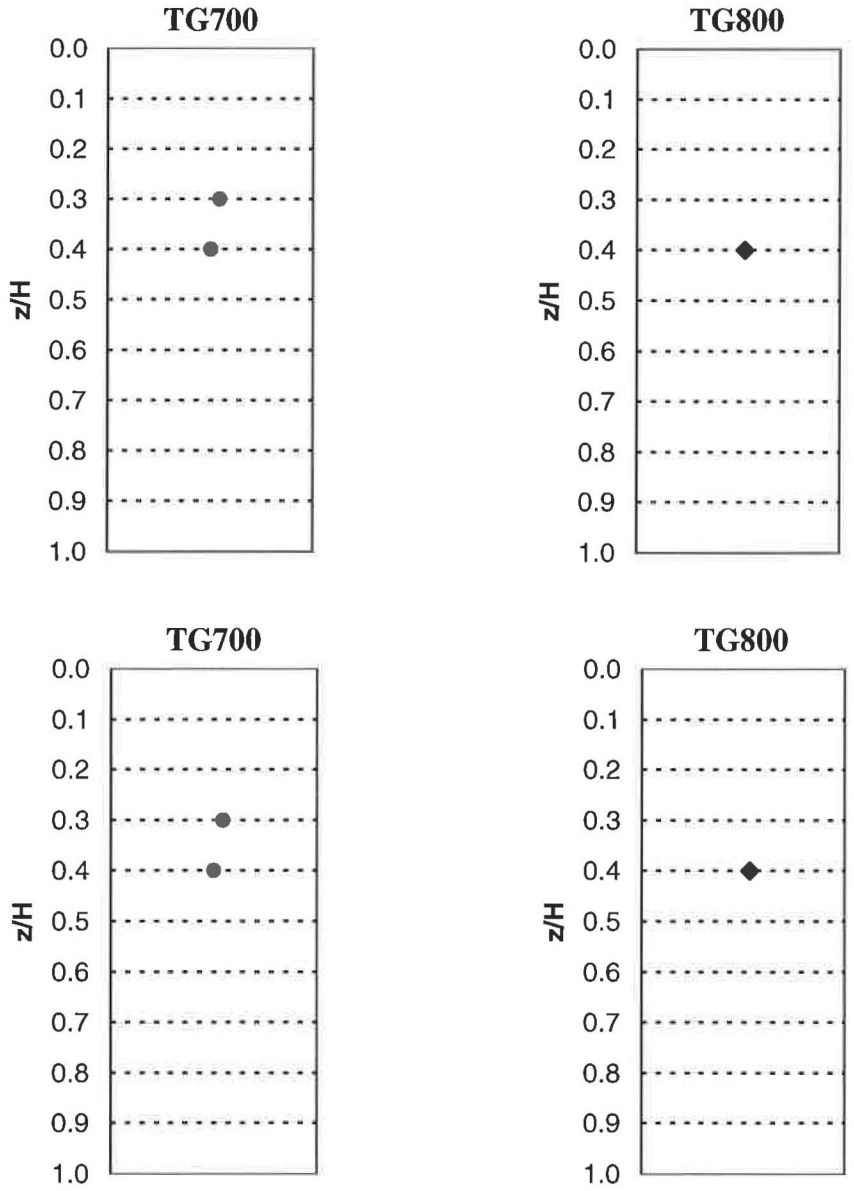


**Figure 4.3** Vertical Cross-sections of the Samples, Along the Machine Direction, Showing Tear Locations found after Failure. Dotted Lines are Geotextile Reinforcement Locations.

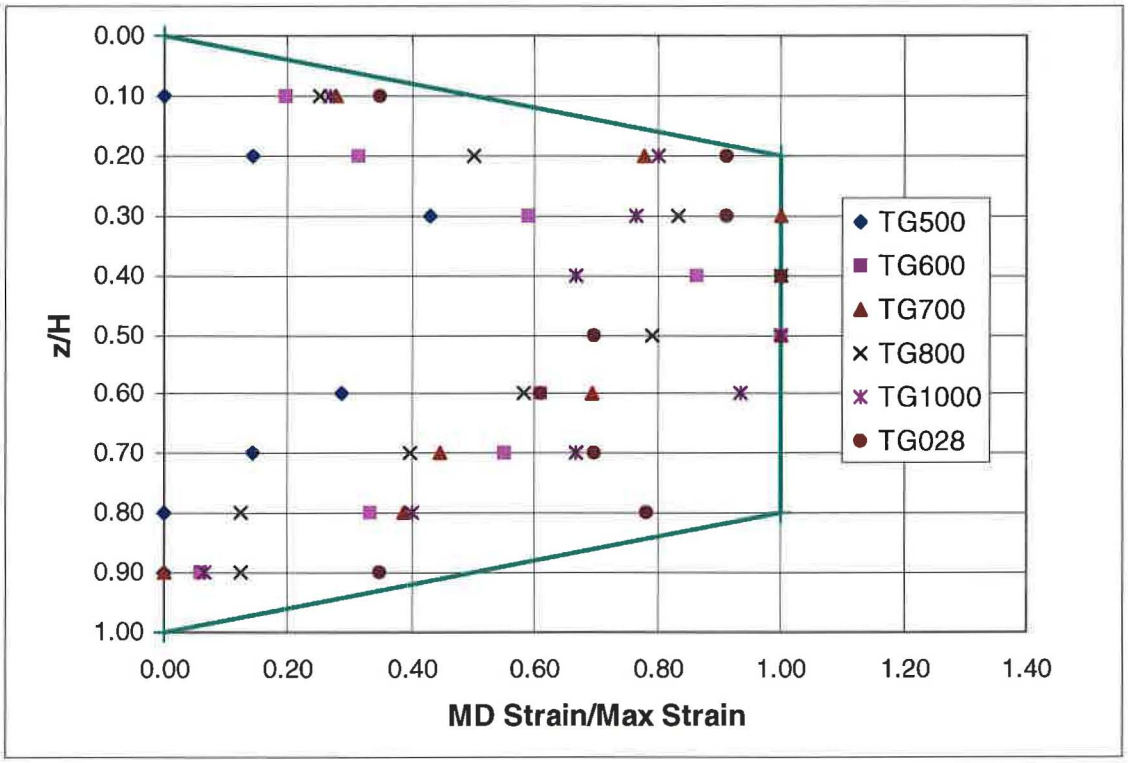


**Figure 4.4** The Strain Distribution Curve from Normalized Geotextile Strains

The boundary lines were named the strain distribution curve. It linearly increases from zero to unity at z/H ranging from 0 to 0.20. It is equal to 1.0 at z/H of 0.20 to 0.80 after which it linearly decreases to zero at z/H equal to 1.0. The value obtained from the strain distribution curve will be called the strain distribution factor (SDF) as it is used in the calculation of the required maximum tensile strength of the reinforcement, Tmax.

The normalized strains appeared to be maximum and symmetric about the middle of the sample then taper off at the ends. This implies that the stresses in the reinforcement are largest for the middle layers and decreasing at the ends. The stresses in the reinforcement increased as the depth increases due to increasing overburden pressure. However, the normalized strains show that the stresses would start to decrease at z/H greater than 0.80.

## V. DATA FROM WALLS IN LITERATURE

To help in the analysis of strains in the reinforcement, data from existing walls were gathered and analyzed. Walls with available strain data were selected from walls whose reinforcements were instrumented with strain gages and/or extensometers. The majority of the data used in the analyses were from Allen and Bathurst (2001). Available literature from individual walls was also utilized.

### 5.1 Walls

Seventeen geosynthetic reinforced walls were selected, based on their available strain data. All the walls were reinforced with geosynthetics (Allen and Bathurst, 2001; Wu et al., 2001). Four different facing types were represented: wrapped face, incremental panel, segmental blocks, and propped panels. The backfill properties of the walls are given in Table 5.2 (Allen and Bathurst, 2001; Wu et al., 2001).

### 5.1.1 Wrapped face walls

Two wrapped face walls were used in the study: the Rainier Avenue Wall of the Washington State Department of Transportation (WSDoT) in Seattle, WA, and the Royal Military College of Canada (RMCC) Wall 1 in Ontario, Canada.

**Table 5.1** Existing Walls used in Study

| Wall Name | Height (ft) | Reinforcement | Facing |
|---|---|---|---|
| Algonquin Wall 1 | 20 | GG – HDPE | Concrete Panel |
| Algonquin Wall 2 | 20 | GG - PET | Modular Block |
| Black Hawk Abutment | 20.7 | GT (W) - PP | Rock Facing |
| Fredericton Wall | 20 | GG – HDPE | Concrete Panel |
| Rainier Ave. Wall | 41.3 | GT(W) – PP/PET | Wrapped Face |
| RMCC Wall 1 | 10 | GG – PP | Wrapped Face |
| RMCC Wall 2 | 10 | GG – HDPE | Timber – Incremental |
| RMCC Wall 3 | 10 | GG – PP | Aluminum – Incremental |
| RMCC Wall 4 | 10 | GG – HDPE | Timber – Full Height |
| RMCC Wall 5 | 10 | GG - PP | Aluminum – Full Height |
| Tanque Verde Wall | 15.25 | GG - HDPE | Concrete Panel |

GG – Geogrid; GT (W) – Woven Geotextile; PP – Polypropylene; PET – Polyethylene; HDPE – High Density Polyethylene

**Table 5.2** Backfill Properties

| Wall Name | Backfill | Unit Weight (pcf) | Design $\phi$ (°) |
|---|---|---|---|
| Algonquin Wall 1 | Well Graded Gravelly Sand | 130.00 | 40° |
| Algonquin Wall 2 | Well Graded Gravelly Sand | 130.00 | 40° |
| Black Hawk Abutment | SM-SC | 124.00 | 31° |
| Fredericton Wall | Coarse Sand with Gravel | 130.00 | 40° |
| Rainier Ave. Wall | Well Graded Gravelly Sand | 134.00 | 36° |
| RMCC Wall 1 | Sand with some Gravel | 112.00 | 40° |
| RMCC Wall 2 | Sand with some Gravel | 114.48 | 40° |
| RMCC Wall 3 | Sand with some Gravel | 114.48 | 40° |
| RMCC Wall 4 | Sand with some Gravel | 114.48 | 40° |

| | | | |
|---|---|---|---|
| RMCC Wall 5 | Sand with some Gravel | 114.48 | 40° |
| Tanque Verde Wall | Well Graded Gravelly Sand | 125.00 | 34° |

The 41.3 ft high Rainier Avenue Wall had a wrapped facing and was reinforced with four different woven geotextiles of varying tensile strengths spaced 1.25 ft apart.

The reinforcement strains for the wrapped face walls are tabulated in Table 5.3 at each reinforcement location z/H where z is the depth of the reinforcement from the top of the wall and H is the height of the wall. The reinforcement used for the Rainier Avenue Wall had ultimate tensile strengths, $T_{ult}$, ranging from 2124 lb/ft at the top to 12748 lb/ft at the bottom (Table 5.3). The weakest geotextiles exhibited the highest strains at 1.14% without surcharge and 1.5% with 2331 psf surcharge. The strongest geotextile had the lowest strains at 0.52% and 0.62% with and without surcharge, respectively.

**Table 5.3** Reinforcement Strains for Wrapped Face Walls

| Wall Name | z/H | $T_{ult}$ (lb/ft) | Strain (%) | Strain/Max Strain |
|---|---|---|---|---|
| Rainier Avenue Wall (no surcharge) | 0.25 | 2124 | 1.14 | 1.00 |
| | 0.52 | 4250 | 0.92 | 0.81 |
| | 0.76 | 6305 | 0.84 | 0.74 |
| | 0.91 | 12748 | 0.52 | 0.46 |
| Rainier Avenue Wall (with surcharge) | 0.25 | 2124 | 1.50 | 1.00 |
| | 0.52 | 4250 | 1.06 | 0.71 |
| | 0.76 | 6305 | 1.06 | 0.71 |
| | 0.91 | 12748 | 0.62 | 0.41 |
| RMCC Wall 1 | 0.21 | 1096 | 1.97 | 0.74 |
| | 0.47 | 1096 | 2.66 | 1.00 |
| | 0.74 | 1096 | 1.25 | 0.47 |
| | 1.00 | 1096 | 0.20 | 0.08 |

The RMCC Wall 1 was a 10 ft high wrapped face wall constructed at the RMCC Retaining Wall Test Facility reinforced with a biaxial geogrid at 2.46 ft vertical spacing (Bathurst et al., 1988; Bathurst, 1993). Uniformly graded washed sand with some gravel (unit weight of 112 pcf) was used as a backfill. Strains in the reinforcement were determined using strain gages and extensometers attached to the ribs of the geogrid. Displacement transducers recorded horizontal movements of the facing.

The reinforcement used for RMCC Wall 1 had an ultimate tensile strength of 1096 lb/ft. Maximum strain recorded for the wall reinforcement was 2.66% at the middle layer (Table 5.3).

### 5.1.2 Incremental panel walls

Three walls with incremental panel facing were used in the study: the Algonquin Wall 1 built by the Federal Highway Administration (FHWA) in Algonquin, Illinois, and two walls built by RMCC in Ontario, Canada, with timber and aluminum panels as facings.

Table 5.4 contains the reinforcement strains measured from the incremental panel facing walls. The Algonquin Wall 1 reinforcement had an ultimate strength, Tult, of 4647 lb/ft. Data shows that the middle layers of the wall strained the most. A maximum strain of 0.76% was recorded for the wall.

RMCC Walls 2 and 3 were built at the RMCC Retaining Wall Test Facility (Bathurst, et al, 1987).

**Table 5.4** Reinforcement Strains for Incremental Panel Facing Walls

| Wall Name | z/H | $T_{ult}$ (lb/ft) | Strain (%) | Strain/Max Strain |
|---|---|---|---|---|
| Algonquin Wall 1 | 0.20 | 4647 | 0.35 | 0.46 |
| | 0.41 | 4647 | 0.71 | 0.93 |
| | 0.69 | 4647 | 0.76 | 1.00 |
| | 0.82 | 4647 | 0.74 | 0.97 |
| | 0.93 | 4647 | 0.18 | 0.24 |
| RMCC Wall 2 (no surcharge) | 0.17 | 4592 | 0.04 | 0.11 |
| | 0.42 | 4592 | 0.27 | 0.79 |
| | 0.67 | 4592 | 0.32 | 0.94 |
| | 0.92 | 4592 | 0.34 | 1.00 |
| RMCC Wall 2 (with surcharge) | 0.17 | 4592 | 0.80 | 1.00 |
| | 0.42 | 4592 | 0.79 | 0.99 |
| | 0.67 | 4592 | 0.60 | 0.75 |
| | 0.92 | 4592 | 0.53 | 0.66 |
| RMCC Wall 3 (no surcharge) | 0.17 | 822 | 0.18 | 0.30 |
| | 0.42 | 822 | 0.60 | 1.00 |
| | 0.67 | 822 | 0.35 | 0.58 |
| | 0.92 | 822 | 0.45 | 0.75 |
| RMCC Wall 3 (with surcharge) | 0.17 | 822 | 4.00 | 0.96 |
| | 0.42 | 822 | 4.15 | 1.00 |
| | 0.67 | 822 | 1.20 | 0.29 |
| | 0.92 | 822 | 0.42 | 0.10 |

RMCC Wall 2 had reinforcements with ultimate tensile strengths, Tult, of 4592 lb/ft while Wall 3 had weaker reinforcements with ultimate tensile strengths of only 822 lb/ft (Table 5.4). The strains recorded for Wall 2 were all below 1%. The maximum strain recorded was at 0.80% when the wall was loaded with a 1044 psf surcharge (Bathurst and Benjamin, 1990; Bathurst, 1993). The reinforcement strains for Wall 3 were all less than 1% without the surcharge but strains of up to 4.15% were reached when the wall was loaded with a 1462 psf surcharge (Bathurst, 1993).

### 5.1.3 Segmental blocks walls

Two walls were used in the study: the Algonquin Wall 2 built by the Federal Highway Administration (FHWA) in Algonquin, Illinois and the Black Hawk Abutment at Black Hawk, CO.

The Algonquin Wall 2 was a 20 ft high wall reinforced with geogrids at various spacing and with gravelly sand (unit weight of 130 pcf) as backfill. The Black Hawk Abutments support the Bobtail Road Bridge constructed over a creek. The abutments were reinforced with woven geotextiles at 1ft spacing, which were held in place between the blocks of rock that also served as facing.

**Table 5.5** Reinforcement Strains for Segmental Block Facing Walls

| Wall Name | z/H | $T_{ult}$ (lb/ft) | Strain (%) | Strain/Max Strain |
|---|---|---|---|---|
| Algonquin Wall 2 (no surcharge) | 0.13 | 2686 | 0.20 | 0.29 |
| | 0.43 | 2686 | 0.42 | 0.64 |
| | 0.66 | 2686 | 0.51 | 0.73 |
| | 0.85 | 2686 | 0.70 | 1.00 |
| | 0.95 | 2686 | 0.19 | 0.27 |

| | | | | |
|---|---|---|---|---|
| Algonquin Wall 2 (with surcharge) | 0.13 | 2686 | 0.42 | 0.38 |
| | 0.43 | 2686 | 0.95 | 0.86 |
| | 0.66 | 2686 | 1.00 | 1.00 |
| | 0.85 | 2686 | 0.95 | 0.86 |
| | 0.95 | 2686 | 0.25 | 0.23 |
| Black Hawk Abutment | 0.10 | 4798 | 0.18 | 1.00 |
| | 0.19 | 4798 | 0.04 | 0.22 |
| | 0.24 | 4798 | 0.06 | 0.33 |

### 5.1.4 Propped panel walls

The study used these four walls: the Fredericton Wall in New Brunswick, Canada; the Tanque Verde Wall in Tucson, Arizona; and two walls from RMCC in Ontario, Canada.

The Fredericton Wall was a 20 ft high wall reinforced with geogrids at 2 ft vertical spacing (Knight and Valsangkar, 1993).

The Tanque Verde Walls were constructed as grade separation for the Tanque Verde – Wrightstown – Pantano Roads. The walls, up to 20 ft high, were reinforced with geogrids at various vertical spacing. (Berg et al., 1986; Bright et al., 1994).

The reinforcements used for the Fredericton and Tanque Verde Walls had the same ultimate tensile strength, $T_{ult}$, at 5003 lb/ft (Table 5.6). The measured strains were very low with a maximum value of only 0.50%.

**Table 5.6** Reinforcement Strains for Propped or Full-Height Panel Facing Walls

| Wall Name | z/H | $T_{ult}$ (lb/ft) | Strain (%) | Strain/Max Strain |
|---|---|---|---|---|
| Fredericton Wall | 0.40 | 5003 | 0.43 | 0.86 |
| | 0.80 | 5003 | 0.50 | 1.00 |
| Tanque Verde Wall | 0.25 | 5003 | 0.18 | 0.55 |
| | 0.71 | 5003 | 0.33 | 1.00 |
| | 0.90 | 5003 | 0.25 | 0.76 |
| RMCC Wall 4 (no surcharge) | 0.17 | 4592 | 0.04 | 1.00 |
| | 0.42 | 4592 | 0.02 | 0.50 |
| | 0.67 | 4592 | 0.02 | 0.50 |
| | 0.92 | 4592 | 0.01 | 0.25 |
| RMCC Wall 4 (with surcharge) | 0.17 | 4592 | 0.50 | 1.00 |
| | 0.42 | 4592 | 0.49 | 0.98 |
| | 0.67 | 4592 | 0.33 | 0.66 |
| | 0.92 | 4592 | 0.22 | 0.44 |
| RMCC Wall 5 (no surcharge) | 0.17 | 822 | 0.40 | 0.95 |
| | 0.42 | 822 | 0.34 | 0.81 |
| | 0.67 | 822 | 0.26 | 0.62 |
| | 0.92 | 822 | 0.42 | 1.00 |
| RMCC Wall 5 (with surcharge) | 0.17 | 822 | 2.93 | 0.84 |
| | 0.42 | 822 | 3.47 | 1.00 |
| | 0.67 | 822 | 2.00 | 0.58 |
| | 0.92 | 822 | 1.45 | 0.42 |

Aside from incremental timber and aluminum panels, the RMCC Retaining Wall Testing Facility also built walls with full-height timber and aluminum panel facings. RMCC Walls 4 and

5 were 10 ft high reinforced with geogrid at 2.46 ft vertical spacing. (Bathurst and Benjamin, 1990).

RMCC Wall 4 was reinforced with a 4592 lb/ft geogrid while Wall 5 reinforcement had a tensile strength of 822 lb/ft (Table 5.6). The reinforcements for Wall 4 did not strain much, exhibiting only 0.50% strain even after the 1044 psf surcharge was applied. The reinforcements for Wall 5 had strains less than 1% without surcharge but strains up to 3.47% were measured after application of the 1671 psf surcharge (Bathurst and Benjamin, 1990).

**5.2 Strain Distribution Curve**

Data derived from instrumentation results of these existing walls were used to evaluate the strains within the wall reinforcements. The reinforcement strains for the walls given in Tables 5.3 to 5.6 were normalized by dividing the individual strains with the maximum strain at each wall. The location of the reinforcement was normalized by dividing its distance from the top, z, with the wall height, H. The normalized strains were plotted with z/H and are shown in Figure 5.1.

The plot shows that the points can be bounded by three lines. The normalized strains are unity for z/H ranging from 0.15 to 0.85. At z/H less than 0.15 and greater than 0.85 the normalized strains are bounded by lines that extend from 1.0 and decreasing linearly to 0.10. There are five points that are not bounded by these lines, representing 9% of the data points.

The three lines make up the strain distribution curve. It linearly increases from 0.10 to 1.0 at z/H ranging from 0 to 0.15. It is equal to 1.0 at z/H of 0.15 to 0.85 after which it linearly decreases to 0.10 at z/H equal to 1.0. Values called the strain distribution factor (SDF) will be derived from this curve based on the reinforcement location and will be used in the calculation of the maximum tensile stress in the reinforcement, Tmax.

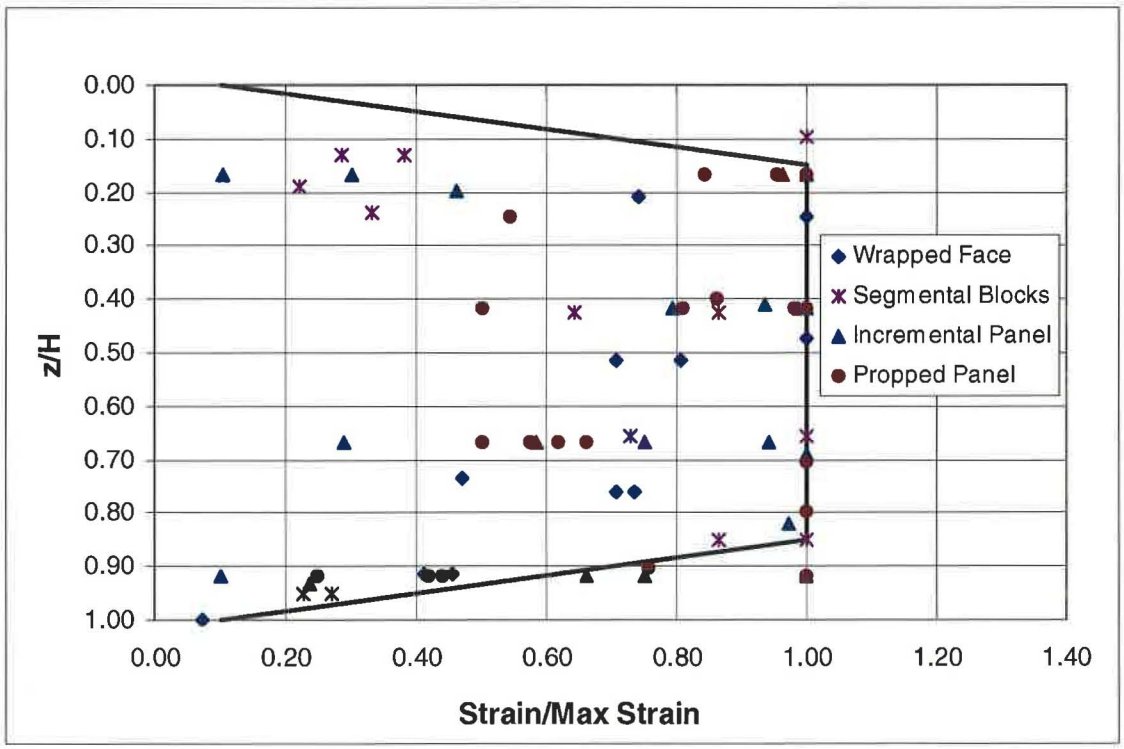


**Figure 5.1** The Strain Distribution Curve from Walls found in Literature

## VI. DEVELOPMENT OF $T_{max\ AU}$ EQUATION

III. The maximum tensile stress in the reinforcement was developed by analysis of the reinforced samples that were tested in the unconfined compression test. The proposed equation, $T_{max\ AU}$, was influenced by the reinforcement spacing, the applied vertical stresses, the strains in the reinforcement and the lateral earth pressure coefficient.

### 6.1 Factors Affecting Strength of Reinforced Soil

Geotextiles are effective if loaded in tension but are not good if loaded in compression. As a reinforced soil is loaded, soil, which cannot take tension, slides on the reinforcement. The friction between the two materials causes the reinforcement to stretch and mobilizes its strength. A reinforced soil derives its strength from these mobilized forces.

The edges of the sample reach failure first. This was evident in the tested samples. It was observed that as load was applied on the reinforced sample, the soil between the layers of reinforcement bulged until they eventually fail and fall out. At or near the reinforcement, however, the friction at the soil-reinforcement interface caused an increase in the confining pressure that holds and keeps the soil from falling out. The closer the reinforcement spacing, the larger the friction at the interface.

The spacing of the reinforcement influences the activation of the reinforcement tensile strength (Vulova and Leshchinsky, 2003).

The strength of a reinforced soil comes from the mobilized tensile strength of the reinforcement (Juran, et al., 1988; Chandrasekaran, et al., 1989). As the wide width tensile strength of the reinforcement increases, the strength of the reinforced sample also increases (Figure 5.1).

### 6.2 Prediction of $T_{max\ AU}$

The maximum tensile force in a layer of reinforcement, $T_{max\ AU}$, is equal to the horizontal stress at that layer, $\sigma_h$, multiplied by the tributary vertical distance, $S_v$. It is proposed to be calculated as:

$$T_{max\ AU} = (\sigma_h\ S_v)\ SDF$$

where $\sigma_h = \sigma_v\ K$ and SDF is the strain distribution factor derived from the reinforcement strains. K is the lateral stress coefficient and $\sigma_v$ is the vertical stress on the reinforcement.

### 6.3 Reinforcement Spacing

For a particular layer of reinforcement, it is assumed that the tributary vertical distance, $S_v$, where the reinforcement is considered to be an effective is the bottom half of the soil on top of it and the upper half of the soil below it (Figure 6.1). If the vertical spacing is constant for all layers, the vertical distance where the reinforcement is effective is equal to the vertical spacing. For cases where the vertical spacing between reinforcements is not constant, the vertical distance can be calculated by:

$$S_v = \left(\frac{z_n + z_{n+1}}{2}\right) - \left(\frac{z_n + z_{n-1}}{2}\right)$$

where $z_n$ is the depth of the nth reinforcement layer, $z_{n+1}$ is the depth of the reinforcement below the nth layer, and $z_{n-1}$ is the depth of the reinforcement on top of the nth layer.

### 7.3 Strain Distribution Factor

Strain distribution curves were drawn on normalized strains plotted against z/H for the large unconfined compression samples (Figure 5.4) and for the walls found in literature (Figure 6.1).

The points on the two graphs (Figures 5.4 and 6.1) were combined in a single normalized strain against z/H plot (Figure 6.2). The strain distribution curve from Figure 6.1 was adopted because it included more of the combined points.

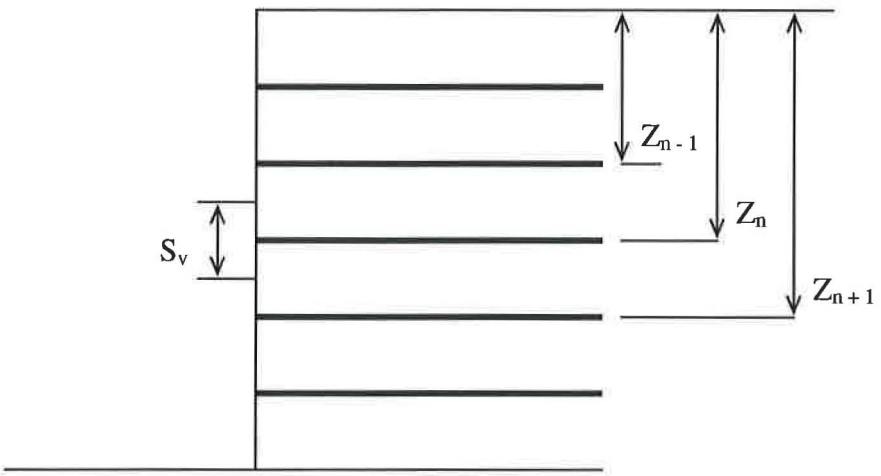


**Figure 6.1** Determination of Reinforcement Spacing, $S_v$

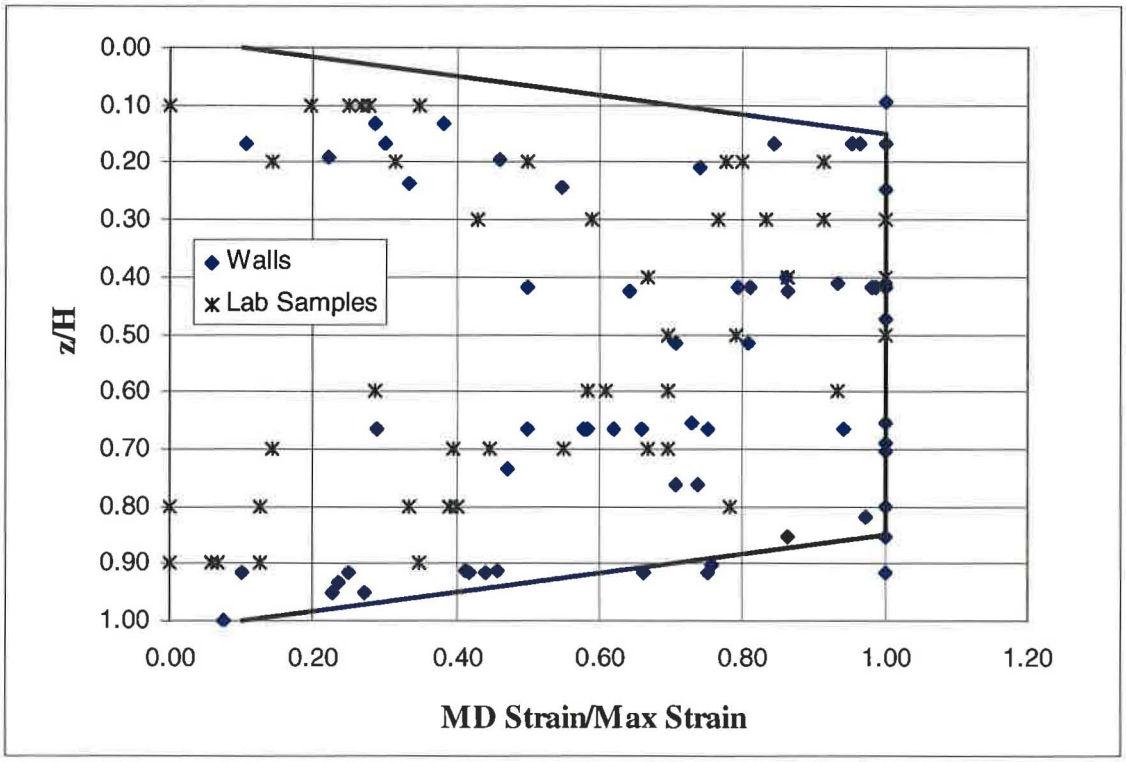


**Figure 6.2** The Strain Distribution Curve used to Determine the Strain Distribution Factor (SDF)

The plot shows that the points can be bounded by three straight lines, as shown. The normalized strains are unity for z/H ranging from 0.15 to 0.85 where z is the depth of the reinforcement measured from the top and H is the height of the sample or wall. At z/H less than 0.15 and greater than 0.85 the normalized strains are bounded by lines that extend from 1.0 and decreasing linearly to 0.10.

The value obtained from the strain distribution curve will be called the strain distribution factor (SDF). It will be used in the calculation of the required maximum tensile strength of the reinforcement, Tmax AU.

**6.4 Vertical Stress**

The vertical stress on a layer of reinforcement is due to the weight of the backfill on top of it and any other applied dead and live loads. The vertical stress, σv, is given as:

$$\sigma_v = \gamma z + q_{DL} + q_{LL}$$

where γ is the total unit weight of the backfill, z is the depth of embedment of the reinforcement, and qDL and qLL are the applied dead and live stresses, respectively.

**6.5 Lateral Earth Pressure Coefficient**

The lateral stress state in a reinforced mass is not known, and not constant. Chandrasekaran et al. (1989) observed, from triaxial test samples, that the mobilized interface friction is zero at the center and maximum near the periphery, then reduces to zero at the ends. Since the lateral stress state is not constant in a horizontal plane, and changes during loading, the actual lateral stress state has not yet been determined. As loading commences, the lateral stresses decrease, but are never uniform across the specimen. The amount of decrease, and the distribution remain unknown. Hence, an empirical approach is proposed to assign a reasonable value to a lateral earth pressure coefficient that gives good agreement with experimental results using the proposed analysis method.

In order to characterize the stress state with a single number, a lateral earth pressure coefficient that gave good agreement between the predicted and measured behavior was backcalculated.

**6.5.1 Reinforcement strain calculated by deformations**

In order to predict the tensile stresses in the reinforcement it is important that the strains in the reinforcement be determined. The tensile stresses can then be calculated by multiplying the strains by the modulus determined from the wide-width tensile strength test results.

The strains in the reinforcement were determined by two methods. The reinforcement radii along the machine and cross machine directions were measured after the test, and by the use of lateral transducers during the test.

The measured reinforcement radii after the test are presented in Table 6.1. During loading, the reinforcement stretches in the machine direction and contracts in the cross machine direction. To measure the dimensions of the reinforcement after the test, it was necessary that the layer of soil on top of the reinforcement be removed. However, unloading caused the reinforcement to relax. The reinforcement shrank in the machine direction and expanded in the cross machine direction. The measured radii were therefore lesser in the machine direction and more in the cross machine direction than the actual dimensions when the reinforcement was loaded. The amount of shrinkage and expansion was not measured but an estimate can be made from the lateral transducer readings.

**Table 6.1** Measured Reinforcement Dimensions after Loading

| **Machine Direction (inches)** | | | | | | |
|---|---|---|---|---|---|---|
| **z/H** | **TG500** | **TG600** | **TG700** | **TG800** | **TG1000** | **TG028** |
| 0.1 | 30.00 | 30.63 | 31.25 | 30.75 | 30.50 | 30.25 |
| 0.2 | 30.25 | 31.00 | 33.50 | 31.50 | 31.50 | 30.63 |
| 0.3 | 30.75 | 31.88 | 34.50 | 32.50 | 31.44 | 30.44 |
| 0.4 | 31.75 | 32.75 | 34.50 | 33.00 | 31.25 | 30.38 |
| 0.5 | 31.75 | 33.19 | 34.50 | 32.38 | 31.88 | 30.63 |
| 0.6 | 30.50 | 31.94 | 33.13 | 31.75 | 31.75 | 30.38 |
| 0.7 | 30.25 | 31.75 | 32.00 | 31.19 | 31.25 | 30.56 |
| 0.8 | 30.00 | 31.06 | 31.75 | 30.38 | 30.75 | 30.13 |
| 0.9 | 30.00 | 30.19 | 30.00 | 30.38 | 30.13 | 30.00 |
| **Cross Machine Direction (inches)** | | | | | | |
| **z/H** | **TG500** | **TG600** | **TG700** | **TG800** | **TG1000** | **TG028** |
| 0.1 | N/A | 29.94 | 30.13 | 30.25 | 30.13 | 30.50 |
| 0.2 | N/A | 29.56 | 29.75 | 29.50 | 29.50 | 31.31 |
| 0.3 | N/A | 29.13 | 28.63 | 28.63 | 29.50 | 31.31 |
| 0.4 | N/A | 27.75 | 28.00 | 28.13 | 29.88 | 31.44 |
| 0.5 | N/A | 27.06 | 28.75 | 28.75 | 29.88 | 31.00 |
| 0.6 | N/A | 29.50 | 29.88 | 29.38 | 29.88 | 30.88 |
| 0.7 | N/A | 29.75 | 30.25 | 30.00 | 29.75 | 31.00 |
| 0.8 | N/A | 30.25 | 30.25 | 30.25 | 30.25 | 31.13 |
| 0.9 | N/A | 30.00 | 30.00 | 29.88 | 30.38 | 30.50 |

Lateral transducers were mounted on a reference frame and were positioned at the level of the geotextiles: at 1.5 ft, 2.0 ft, 2.5 ft, 3.0 ft, 3.5 ft, and 4 ft from the bottom of the sample. The transducers were positioned 45° from the machine direction. To estimate the strains in the machine and cross machine directions, the actual LVDT readings were adjusted. The lateral transducers that gave reliable results were those at the front of the sample at 2.0ft, 3.0ft, and 4.0ft from the bottom of the sample.

It was assumed that when the layer of soil on top of the reinforcement was removed, the amount of shrinkage/expansion was uniform in all directions. The amount of shrinkage/expansion, $\Delta\varepsilon$, was taken as equal to the difference between the strain from LVDT measurements, $\varepsilon_{LVDT}$, and the mean of the measured machine and cross machine direction strains, $\varepsilon_{Measd\ AVE}$, given as:

$$\Delta\varepsilon = \varepsilon_{LVDT} - \varepsilon_{Measd\,AVE}$$

The strains in the machine direction, $\varepsilon_{MD}$, and the cross machine direction, $\varepsilon_{XMD}$, were then calculated as:

$$\varepsilon_{MD} = \varepsilon_{Measd\,MD} + \Delta\varepsilon$$

$$\varepsilon_{XMD} = \varepsilon_{Measd\,XMD} - \Delta\varepsilon$$

where $\varepsilon_{Measd\ MD}$ is the measured strain in the machine direction and $\varepsilon_{Measd\ XMD}$ is the measured strain in the cross machine direction.

The adjusted strains in the reinforcement for TG600, TG800, TG1000 and TG028 are presented in Table 6.2. The strains from LVDT measurements of TG500 and TG700 were not included in the table because they were considered unreliable.

**Table 6.2** Strains in the Reinforcement (%)

| TG600 | | | | | | |
|---|---|---|---|---|---|---|
| z/H | $\varepsilon_{Measd\ MD}$ | $\varepsilon_{Measd\ XMD}$ | $\varepsilon_{Measd\ AVE}$ | $\varepsilon_{LVDT}$ | $\varepsilon_{MD}$ | $\varepsilon_{XMD}$ |
| 0.2 | 3.33 | -1.46 | 0.94 | 2.34 | 4.74 | -2.86 |
| 0.4 | 9.17 | -7.50 | 0.83 | 7.28 | 15.61 | -13.95 |
| 0.6 | 6.46 | -1.67 | 2.40 | 5.11 | 9.17 | -4.38 |
| **V. TG800** | | | | | | |
| z/H | $\varepsilon_{Measd\ MD}$ | $\varepsilon_{Measd\ XMD}$ | $\varepsilon_{Measd\ AVE}$ | $\varepsilon_{LVDT}$ | $\varepsilon_{MD}$ | $\varepsilon_{XMD}$ |
| 0.2 | 5.00 | -1.67 | 1.67 | 6.88 | 10.21 | -6.88 |
| 0.4 | 10.00 | -6.25 | 1.88 | 18.29 | 26.42 | -22.67 |
| 0.6 | 5.83 | -2.08 | 1.88 | 7.47 | 11.43 | -7.68 |
| **VI. TG1000** | | | | | | |
| z/H | $\varepsilon_{Measd\ MD}$ | $\varepsilon_{Measd\ XMD}$ | $\varepsilon_{Measd\ AVE}$ | $\varepsilon_{LVDT}$ | $\varepsilon_{MD}$ | $\varepsilon_{XMD}$ |
| 0.2 | 5.00 | -1.67 | 1.67 | 8.76 | 12.09 | -8.76 |
| 0.4 | 4.17 | -0.42 | 1.88 | 9.04 | 11.33 | -7.58 |
| 0.6 | 5.83 | -0.42 | 2.71 | 6.74 | 9.87 | -4.45 |
| **VII. TG028** | | | | | | |
| z/H | $\varepsilon_{Measd\ MD}$ | $\varepsilon_{Measd\ XMD}$ | $\varepsilon_{Measd\ AVE}$ | $\varepsilon_{LVDT}$ | $\varepsilon_{MD}$ | $\varepsilon_{XMD}$ |
| 0.2 | 2.08 | 4.38 | 3.23 | 12.82 | 11.67 | 13.97 |
| 0.4 | 1.25 | 4.79 | 3.02 | 11.36 | 9.59 | 13.13 |
| 0.6 | 1.25 | 2.92 | 2.08 | 9.17 | 8.34 | 10.00 |

### 6.6 Tension in the reinforcement

The tensile force in the reinforcement was computed by multiplying the adjusted strains by the initial tangent modulus of the reinforcement from the wide width tensile strength tests. The forces in the weaker direction were calculated. The strength in the machine direction was weaker for TG500, TG600, TG700, TG800 and TG1000. The strength in the cross machine direction was weaker for TG028.

The calculated forced of the reinforcements, T, in the weaker direction are presented in Table 6.3. The modulus, E, is the initial tangent modulus from the wide width tensile strength test.

**Table 6.3** Reinforcement Forces in the Weaker Direction

| **TG600** | | | |
|---|---|---|---|
| **z/H** | **$\varepsilon_{MD}$ (%)** | **E (lb/in)** | **T (lb/ft)** |
| 0.2 | 4.74 | 110 | 62.51 |
| 0.4 | 15.61 | 110 | 206.10 |
| 0.6 | 9.17 | 110 | 121.08 |
| **TG800** | | | |
| **z/H** | **$\varepsilon_{MD}$ (%)** | **E (lb/in)** | **T (lb/ft)** |
| 0.2 | 10.21 | 214 | 134.82 |
| 0.4 | 26.42 | 214 | 348.68 |
| 0.6 | 11.43 | 214 | 150.85 |
| **TG1000** | | | |
| **z/H** | **$\varepsilon_{MD}$ (%)** | **E (lb/in)** | **T (lb/ft)** |
| 0.2 | 12.09 | 238 | 159.63 |
| 0.4 | 11.33 | 238 | 149.58 |
| 0.6 | 9.87 | 238 | 130.22 |
| **TG028** | | | |
| **z/H** | **$\varepsilon_{XMD}$ (%)** | **E (lb/in)** | **T (lb/ft)** |
| 0.2 | 13.97 | 454 | 184.35 |
| 0.4 | 13.13 | 454 | 173.33 |
| 0.6 | 10.00 | 454 | 132.04 |

### 6.6.1 Backcalculation of lateral earth pressure coefficient, K

The maximum tensile force in the reinforcement, Tmax AU, can be calculated as:

$$T_{max\ AU} = (\sigma_v\ K)\ S_v\ SDF$$

where σv is the vertical stress, Sv is the vertical distance and SDF is the strain distribution factor as discussed in previous sections. In calculating the vertical stress, the backfill unit weight was taken as 120 pcf. The peak stresses of the reinforced sample during testing was taken as the equivalent dead and live stresses. The MSE height was taken as equal to 5 ft with the reinforcement spaced 0.5 ft apart. The SDF was taken from the strain distribution curve (Figure 6.2)

The value of Tmax AU was calculated using different K values. The Tmax was compared to the tension force, T, calculated from the strain. The K value that gave a Tmax AU greater than and closer to the tensile force in the reinforcement, T, was considered to be the best choice. The K value was backcalculated by making Tmax AU equal to T and solving for K as:

$$K = \frac{T}{\sigma_v\ S_v\ SDF}$$

Backcalculations using the tensile forces in TG600, TG800, TG1000 and TG028 showed that K needed to be greater than or equal to 0.0807 for Tmax AU to be greater than or equal to T. A K value of 0.09, therefore, can be used in the Tmax AU equation as long as the reinforcement spacing is 6 inches and the backfill friction angle is 40o.

The use of K = 0.09 however is limited to a select backfill with a friction angle of 40o. To find a general equation for K that can be used for different backfill with different friction angles, several Ko and Ka combinations were considered.

## 6.7 $K_o$ - $K_a$

Several investigators have used K's varying from Ko to Ka (Long et al. 1983; NCMA, 1996; Elias and Christopher, 1996; Allen and Bathurst, 2001).

This study used the difference between Ka and Ko. The Rankine equation was used to calculate for Ka,

$$K_a = \tan^2 (45 - \phi/2)$$

where $\phi$ was the soil angle of friction from the direct shear test taken as 40°.

The Jaky equation for Ko (Bowles, 1988) was used where:

$$K_o = \frac{1-\sin\phi}{1+\sin\phi}\left(1+\frac{2}{3}\sin\phi\right)$$

The Tmax AU values using the different Ks were also plotted against z/H for TG800, TG1000 and TG028. The graphs are given in Figures 6.4 to 6.6.

The quantity $K_o - K_a$ yielded the best conservative agreement among the tested reinforced samples. The calculated $T_{max\ AU}$ values were greater than the T values to be considered safe, and at the same time the calculated values were close enough to the reinforcement stresses not to be too conservative. This is not to suggest that the lateral stress state is $K_o - K_a$ throughout the sample. Rather, the quantity $K_o - K_a$ represents a stress state that gives good results for this analysis technique.

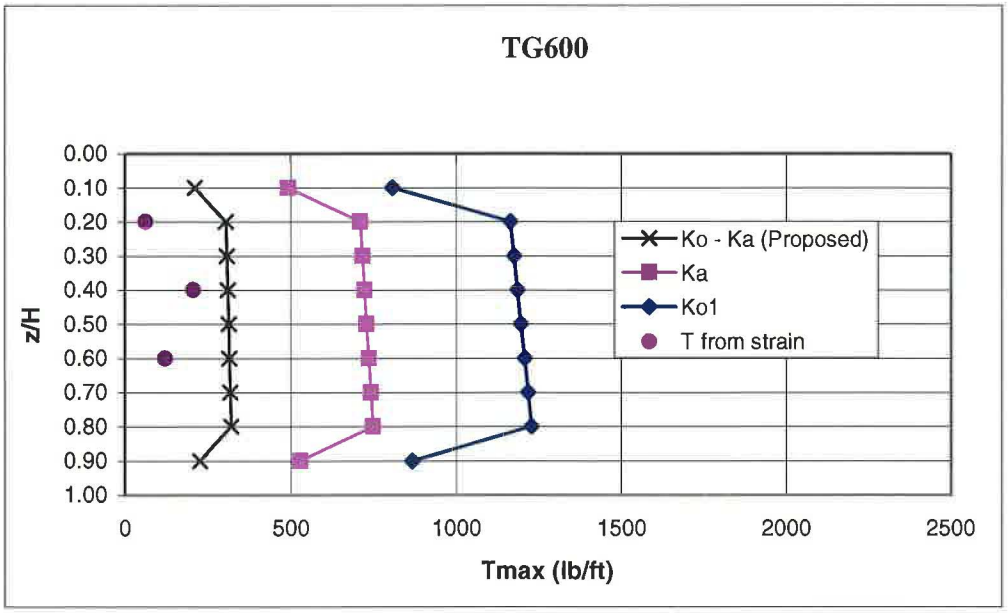


**Figure 6.3** $T_{max\ AU}$ values from various K for TG600

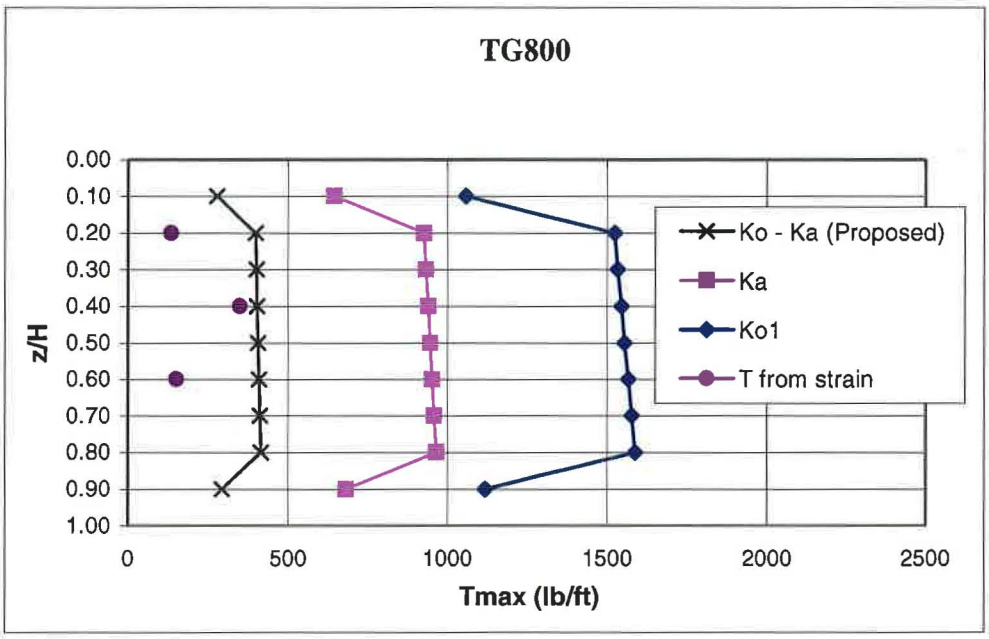


**Figure 6.4** $T_{max\ AU}$ values from various K for TG800

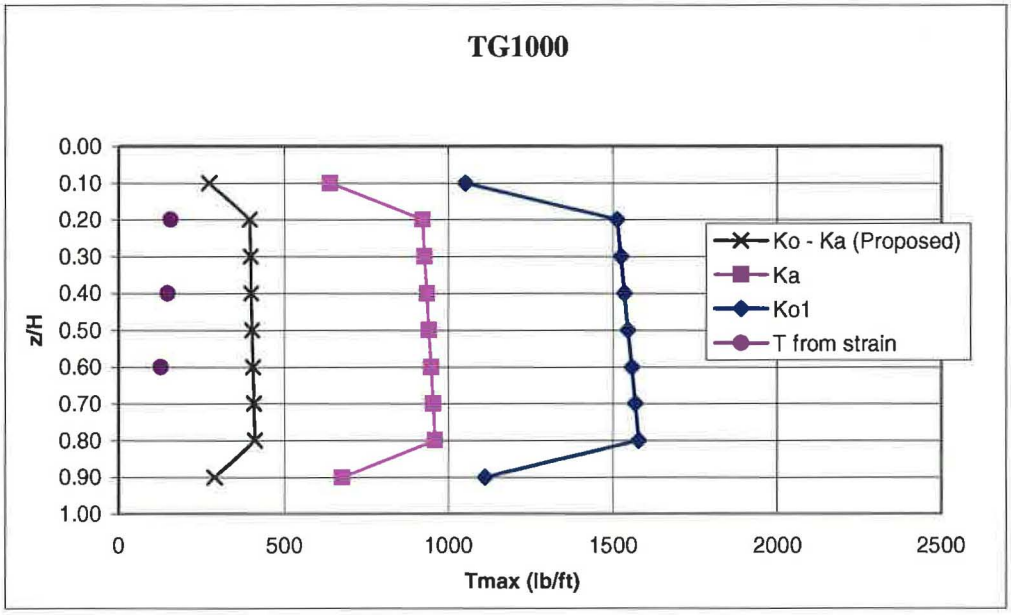


**Figure 6.5** $T_{max\ AU}$ values from various K for TG1000

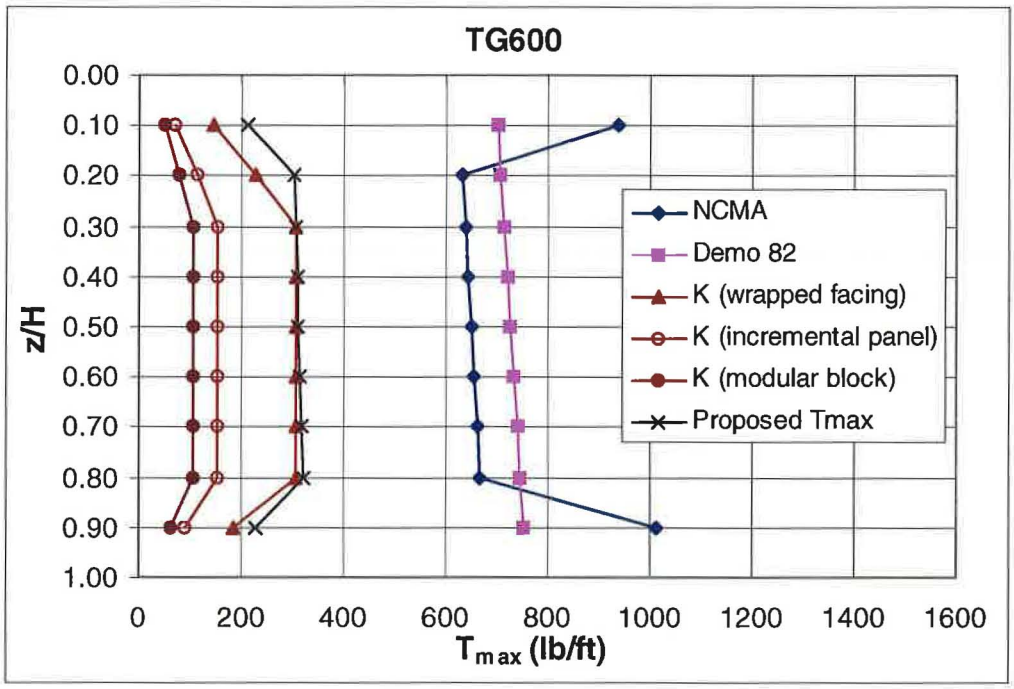


**Figure 7.2** $T_{max}$ values from different methods for TG600

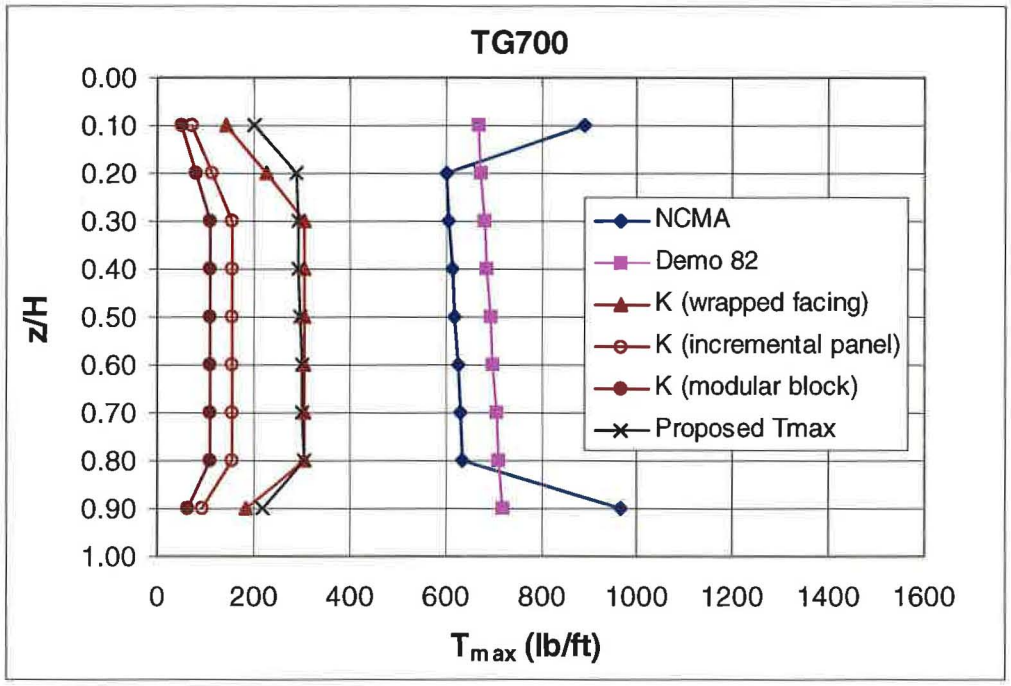


**Figure 7.3** $T_{max}$ values from different methods for TG700

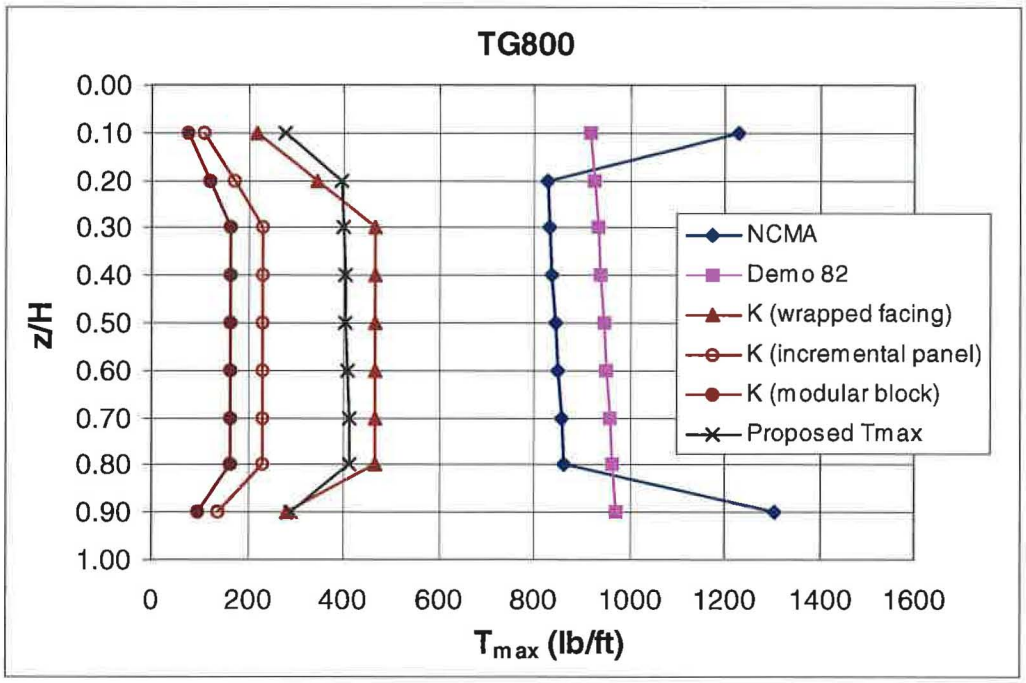


**Figure 7.4** $T_{max}$ values from different methods for TG800

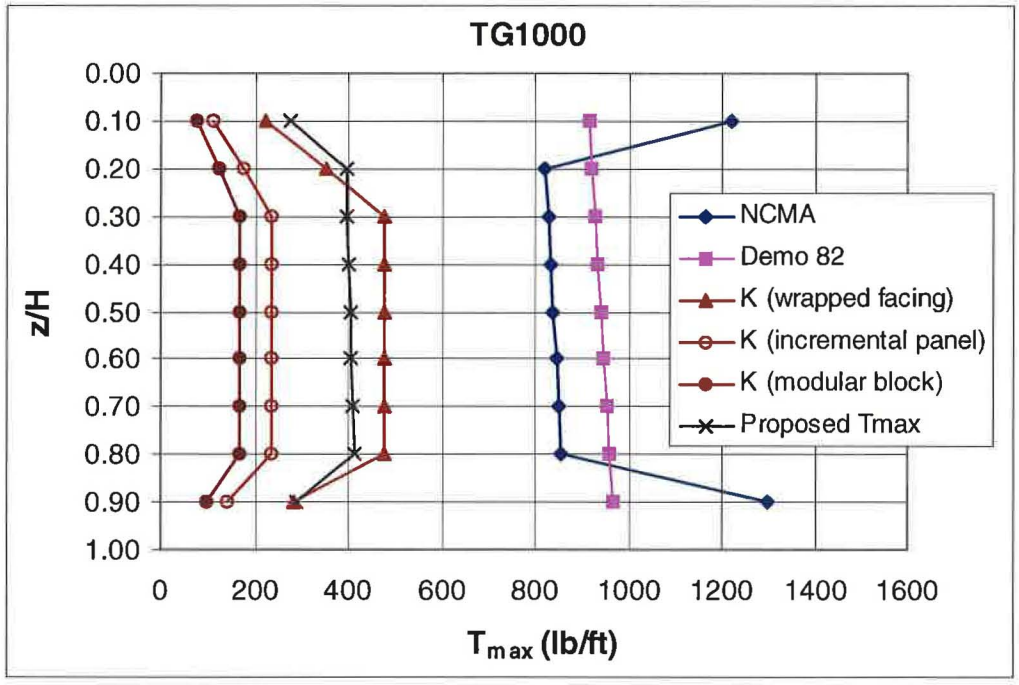


**Figure 7.5** $T_{max}$ values from different methods for TG1000

| | | | | | |
|---|---|---|---|---|---|
| 0.90 | 0.300 | 0.223 | 1.227 | 2.454 | 3.506 |

**Table 7.9** Ratio of $T_{max\ AU}$ with $T_{max}$ from other methods for TG700

| z/H | $\frac{T_{max\ AU}}{T_{max\ DEMO\ 82}}$ | $\frac{T_{max\ AU}}{T_{max\ NCMA}}$ | $\frac{T_{max\ AU}}{T_{max\ K\ STIFFNESS}}$ ($\Phi_{fs} = 1.0$) | $\frac{T_{max\ AU}}{T_{max\ K\ STIFFNESS}}$ ($\Phi_{fs} = 0.5$) | $\frac{T_{max\ AU}}{T_{max\ K\ STIFFNESS}}$ ($\Phi_{fs} = 0.35$) |
|---|---|---|---|---|---|
| 0.10 | 0.300 | 0.224 | 1.396 | 2.793 | 3.990 |
| 0.20 | 0.429 | 0.480 | 1.276 | 2.553 | 3.647 |
| 0.30 | 0.429 | 0.480 | 0.950 | 1.900 | 2.714 |
| 0.40 | 0.429 | 0.480 | 0.959 | 1.918 | 2.740 |
| 0.50 | 0.429 | 0.480 | 0.968 | 1.936 | 2.766 |
| 0.60 | 0.429 | 0.480 | 0.977 | 1.954 | 2.792 |
| 0.70 | 0.429 | 0.480 | 0.986 | 1.973 | 2.818 |
| 0.80 | 0.429 | 0.480 | 0.995 | 1.991 | 2.844 |
| 0.90 | 0.300 | 0.223 | 1.172 | 2.344 | 3.349 |

**Table 7.10** Ratio of $T_{max\ AU}$ with $T_{max}$ from other methods for TG800

| z/H | $\frac{T_{max\ AU}}{T_{max\ DEMO\ 82}}$ | $\frac{T_{max\ AU}}{T_{max\ NCMA}}$ | $\frac{T_{max\ AU}}{T_{max\ K\ STIFFNESS}}$ ($\Phi_{fs} = 1.0$) | $\frac{T_{max\ AU}}{T_{max\ K\ STIFFNESS}}$ ($\Phi_{fs} = 0.5$) | $\frac{T_{max\ AU}}{T_{max\ K\ STIFFNESS}}$ ($\Phi_{fs} = 0.35$) |
|---|---|---|---|---|---|
| 0.10 | 0.300 | 0.224 | 1.266 | 2.532 | 3.617 |
| 0.20 | 0.429 | 0.480 | 1.154 | 2.308 | 3.297 |
| 0.30 | 0.429 | 0.480 | 0.856 | 1.713 | 2.447 |
| 0.40 | 0.429 | 0.480 | 0.862 | 1.725 | 2.464 |
| 0.50 | 0.429 | 0.480 | 0.868 | 1.737 | 2.481 |
| 0.60 | 0.429 | 0.480 | 0.874 | 1.749 | 2.498 |
| 0.70 | 0.429 | 0.480 | 0.880 | 1.761 | 2.515 |
| 0.80 | 0.429 | 0.480 | 0.886 | 1.773 | 2.533 |
| 0.90 | 0.300 | 0.223 | 1.041 | 2.082 | 2.975 |

**Table 7.11** Ratio of $T_{max\ AU}$ with $T_{max}$ from other methods for TG1000

| z/H | $\frac{T_{max\ AU}}{T_{max\ DEMO\ 82}}$ | $\frac{T_{max\ AU}}{T_{max\ NCMA}}$ | $\frac{T_{max\ AU}}{T_{max\ K\ STIFFNESS}}$ ($\Phi_{fs} = 1.0$) | $\frac{T_{max\ AU}}{T_{max\ K\ STIFFNESS}}$ ($\Phi_{fs} = 0.5$) | $\frac{T_{max\ AU}}{T_{max\ K\ STIFFNESS}}$ ($\Phi_{fs} = 0.35$) |
|---|---|---|---|---|---|
| 0.10 | 0.300 | 0.224 | 1.232 | 2.464 | 3.520 |
| 0.20 | 0.429 | 0.480 | 1.123 | 2.247 | 3.209 |
| 0.30 | 0.429 | 0.480 | 0.834 | 1.668 | 2.382 |
| 0.40 | 0.429 | 0.480 | 0.840 | 1.679 | 2.399 |
| 0.50 | 0.429 | 0.480 | 0.845 | 1.691 | 2.416 |
| 0.60 | 0.429 | 0.480 | 0.851 | 1.703 | 2.432 |
| 0.70 | 0.429 | 0.480 | 0.857 | 1.714 | 2.449 |
| 0.80 | 0.429 | 0.480 | 0.863 | 1.726 | 2.466 |
| 0.90 | 0.300 | 0.223 | 1.014 | 2.028 | 2.896 |

**Table 7.12** Ratio of $T_{max\ AU}$ with $T_{max}$ from other methods for TG028

| z/H | $\frac{T_{max\ AU}}{T_{max\ DEMO\ 82}}$ | $\frac{T_{max\ AU}}{T_{max\ NCMA}}$ | $\frac{T_{max\ AU}}{T_{max\ K\ STIFFNESS}}$ ($\Phi_{fs} = 1.0$) | $\frac{T_{max\ AU}}{T_{max\ K\ STIFFNESS}}$ ($\Phi_{fs} = 0.5$) | $\frac{T_{max\ AU}}{T_{max\ K\ STIFFNESS}}$ ($\Phi_{fs} = 0.35$) |
|---|---|---|---|---|---|
| 0.10 | 0.300 | 0.224 | 0.985 | 1.969 | 2.813 |
| 0.20 | 0.429 | 0.480 | 0.897 | 1.794 | 2.562 |
| 0.30 | 0.429 | 0.480 | 0.665 | 1.330 | 1.900 |
| 0.40 | 0.429 | 0.480 | 0.669 | 1.338 | 1.912 |
| 0.50 | 0.429 | 0.480 | 0.673 | 1.346 | 1.923 |
| 0.60 | 0.429 | 0.480 | 0.677 | 1.355 | 1.935 |
| 0.70 | 0.429 | 0.480 | 0.681 | 1.363 | 1.947 |
| 0.80 | 0.429 | 0.480 | 0.685 | 1.371 | 1.959 |
| 0.90 | 0.300 | 0.223 | 0.805 | 1.609 | 2.299 |

**Table 7.13** Average Ratio of $T_{max\ AU}$ with $T_{max}$ from other methods

| Reinf. | $\frac{T_{max\ AU}}{T_{max\ DEMO\ 82}}$ | $\frac{T_{max\ AU}}{T_{max\ NCMA}}$ | $\frac{T_{max\ AU}}{T_{max\ K\ STIFFNESS}}$ ($\Phi_{fs} = 1.0$) | $\frac{T_{max\ AU}}{T_{max\ K\ STIFFNESS}}$ ($\Phi_{fs} = 0.5$) | $\frac{T_{max\ AU}}{T_{max\ K\ STIFFNESS}}$ ($\Phi_{fs} = 0.35$) |
|---|---|---|---|---|---|
| TG500 | 0.429 | 0.480 | 1.225 | 2.449 | 3.499 |
| TG600 | 0.429 | 0.480 | 1.128 | 2.257 | 3.224 |
| TG700 | 0.429 | 0.480 | 1.076 | 2.151 | 3.073 |
| TG800 | 0.429 | 0.480 | 0.965 | 1.931 | 2.759 |
| TG1000 | 0.429 | 0.480 | 0.940 | 1.880 | 2.686 |
| TG028 | 0.429 | 0.480 | 0.749 | 1.497 | 2.139 |

## 7.2 Implications for Design

### 7.2.1 Factor of safety against rupture

The ultimate tensile strength of a geosynthetic is determined by the wide-width tensile strength test (ASTM D4595). The wide-width tensile strengths of the reinforcements, $T_{ult}$, are given in Table 7.14. However, the behavior of a geotextile when it is loaded in air is different when it is between backfill. The friction at the soil reinforcement interface as the soil slides when the sample is loaded causes the geotextile to stretch and mobilizes its tensile strength. How much the geotextile stretches in these tests before it breaks when it is between backfill was not measured and is not known. Inspection after the test showed that the sample reinforced with TG600 had 2 layers of ruptured reinforcement (Table 7.14) while TG800 had 1 layer. The wide width tensile strength test elongation at failure (Table 4.4) of TG600 was 135% while TG800 failed at 123% elongation. The estimated maximum strain during the test of TG600 and TG800 from measured and LVDT strains (Table 7.2) were only 15% and 26%, respectively. That means the reinforcements were torn at strains much less than their wide width tensile test failure strains.

The ratios of the reinforcement wide-width tensile strengths, $T_{ult}$, with the $T_{max\ AU}$ values are shown in Table 7.14. The samples reinforced with TG500, TG600, TG700 and TG800 have a maximum of 6 layers to a minimum of 1 layer of ruptured reinforcement and have $T_{ult}/T_{max\ AU}$ ratios ranging from 2.49 to 3.26. The samples reinforced with TG1000 and TG028 had layers of stretched reinforcement but no layer was ruptured during loading. The ratio of $T_{ult}/T_{max\ AU}$ for

TG1000 and TG028 were 3.34 and 3.18, respectively. The ratios seem to indicate that the minimum wide width tensile strength, $T_{ult}$, of a reinforcement needed to ensure that no layer will tear is about $3.5T_{max\ AU}$. The factor of safety against rupture, $FS_{rupture}$, can therefore be taken as equal to 3.50.

**Table 7.14** Ratio of ultimate tensile strength $T_{ult}$ with the proposed $T_{max\ AU}$

| Geotextile Reinf. | $T_{ult}$ (WW Test) lb/ft | $T_{max\ AU}$ lb/ft | $T_{ult}/T_{max\ AU}$ ($FS_{rupture}$) | No. of torn layers |
|---|---|---|---|---|
| TG500 | 612 | 245.99 | 2.49 | 6 |
| TG600 | 960 | 320.07 | 3.00 | 2 |
| TG700 | 996 | 305.16 | 3.26 | 1 |
| TG800 | 1272 | 413.72 | 3.07 | 1 |
| TG1000 | 1375 | 411.39 | 3.34 | 0 |
| TG028 | 1490 | 468.23 | 3.18 | 0 |

### 7.2.2 Effective Area

As the sample is tested in unconfined compression, spalling occurs (Figure 4.13). The soil between two layers of reinforcement starts to bulge, reach failure and eventually falls off. This loss of soil at the edges of the sample causes a reduction in the effective area that carries the load. To check how much reduction occurs in the effective area, the vertical stress, $\sigma_v$, when the reinforcement is at its ultimate strength, $T_{ult}$, was backcalculated (Table 7.15):

$$\sigma_v = \frac{T_{ult}}{S_v (K_o - K_a)(SDF)}$$

where $S_v$ is 0.5 ft, SDF is 1.0 and $(K_o - K_a)$ is 0.0932. The effective area, A', was then calculated by dividing the peak force recorded during loading by the loadcell, F, by the vertical stress, $\sigma_v$:

$$A' = \frac{F}{\sigma_v}$$

Calculations showed that the effective area ranged from 1.46 $ft^2$ to 1.82 $ft^2$ (Table 7.15). The initial area of the sample was 4.91 $ft^2$. Calculations showed that area reduction ranged from about 63% to 70% with an average value of about 68%. This suggests that during unconfined compression testing of reinforced soil samples, when the tensile stresses on the reinforcement are equal to $T_{ult}$, only about 32% of the initial area is effective in carrying the applied load. The vertical stresses at the edges are zero and maximum on only 32% of the initial area.

The average Tult/Tmax AU ratio is about 3.1 (Table 7.14). The use of Tult to calculate the vertical stress, instead of Tmax AU, increases the vertical stress by a factor of three, which in turn, reduces the effective area to a third of its initial value.

In an unconfined compression test, the volume is assumed to be constant during the test. As the sample is loaded, the corrected area, Acorrected, becomes a function of the vertical strain, ε, and is given as:

$$A_{corrected} = \frac{A_o}{1 - \varepsilon}$$

where $A_o$ is the initial area.

The vertical stress on a sample in an unconfined compression test is calculated by dividing the applied force by the corrected area. Thus, the vertical stresses on the reinforced samples (Figure 5.1) were calculated by dividing the measured forces with the corrected areas.

Reduced areas affect the calculations by increasing the vertical stress for the same amount of applied vertical force. This increase in vertical stress results to an increase in the tensile stress in the reinforcement and requires that a stronger reinforcement be used which translates to a higher cost of reinforcement.

However, reinforced abutments normally have facings that confine the backfill and prevent spalling. Therefore, the actual effective areas of reinforced abutments are actually larger and suggest that abutments with the same reinforcement and spacing as the unconfined samples can carry more load than the tested unconfined samples.

**Table 7.15** Effective area during unconfined compression testing

| Geotextile Reinf. | $T_{ult}$ (lb/ft) | $\sigma_v$ (psf) | F (kips) | Effective Area ($ft^2$) | %Area Reduction |
|---|---|---|---|---|---|
| TG500 | 612 | 13133 | 23.93 | 1.82 | 62.92 |
| TG600 | 960 | 20601 | 31.97 | 1.55 | 68.42 |
| TG700 | 996 | 21373 | 31.14 | 1.46 | 70.26 |
| TG800 | 1272 | 27296 | 43.28 | 1.59 | 67.61 |
| TG1000 | 1375 | 29506 | 44.29 | 1.50 | 69.44 |
| TG028 | 1490 | 31794 | 51.32 | 1.60 | 67.40 |
| | | | Average | 1.59 | 67.68 |

### 7.2.3 Reinforced friction angle

To determine the friction angle of a reinforced soil, the Mohr circles of the reinforced samples were plotted (Figure 7.7). Lines passing through the backfill apparent cohesion (0.6 ksf from direct shear test) and tangent to the circles were drawn as shown in Figure 7.7. The angles the lines make with the horizontal were then measured and considered as the reinforced friction angle, $\phi_{reinf}$ (Figure 7.7). The reinforced friction angle increased as the tensile strength of the reinforcement increased (Figures 7.7 to 7.8 and Table 7.16).

The reinforced friction angle of the sample, $\phi_{reinf}$, reinforced with TG500 spaced 12 inches apart (TG500-12 in Table 7.16) was 42.5° which was almost equal to the backfill friction angle, $\phi$ = 40°. The sample reinforced with TG500 at 12 inches spacing failed at a low compressive stress. The sample reached peak strength of about 2.7 ksf at 1.5% strain (Figure 5.1) then dropped sharply to less than half its peak. Inspection of the reinforcement after loading showed no rupture in any of the layers indicating that the reinforcement may not have been mobilized to contribute any strength to the sample. The almost equal values of the reinforced friction angle ($\phi_{reinf}$ = 42.5°) and the backfill friction angle ($\phi$ = 40°) for the sample reinforced with TG500 at 12 inches spacing, was another indication that the reinforcement was not effective and the reinforcement tensile strength was barely mobilized during loading. The reinforced friction angle, $\phi_{reinf}$, for the samples with reinforcement spaced 6 inches apart were higher than that of the backfill and ranged from 62° to 75° (Table 7.16).

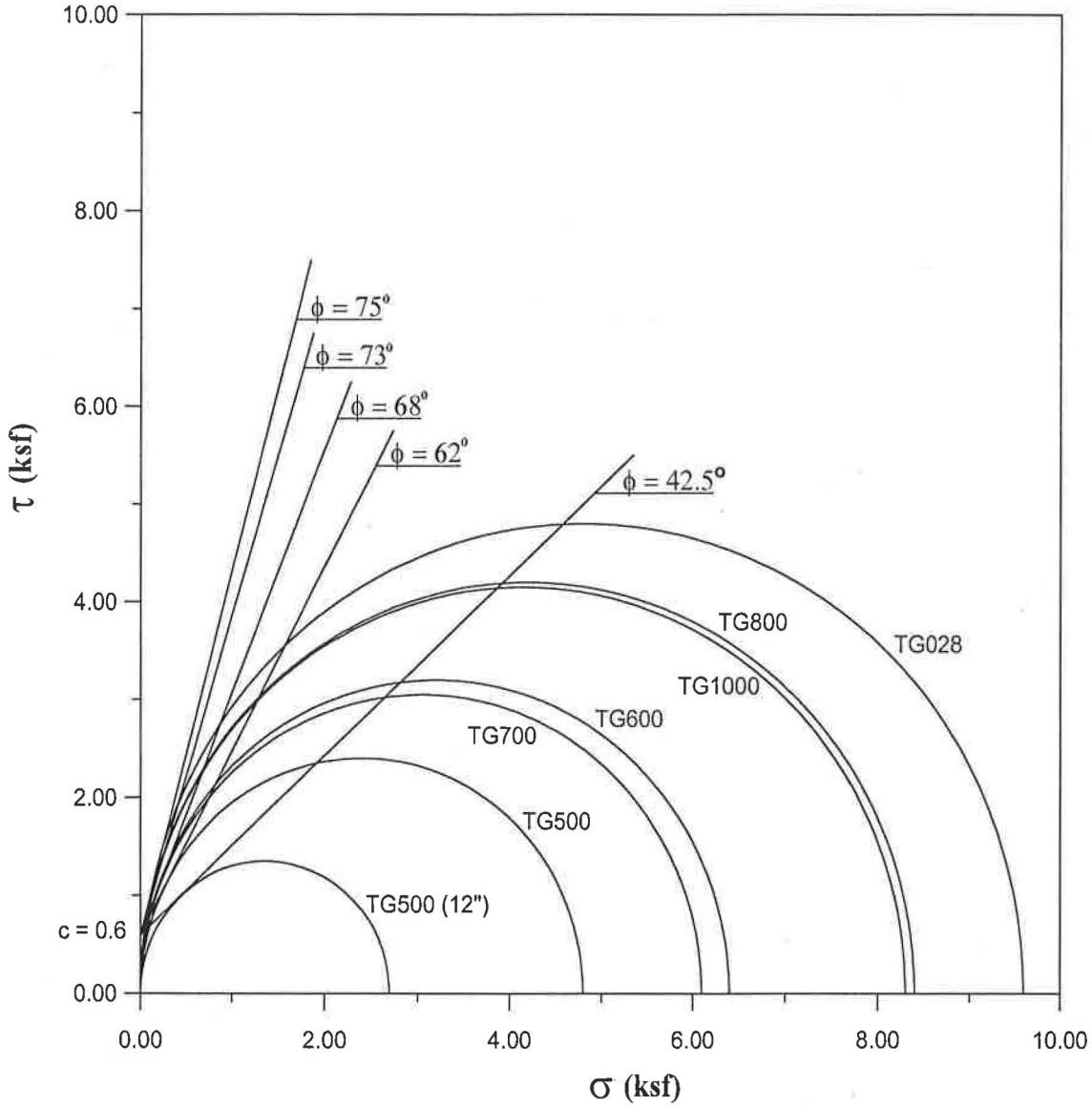


**Figure 7.7** Mohr Circles and $\phi_{reinf}$ for Reinforced Soil Samples

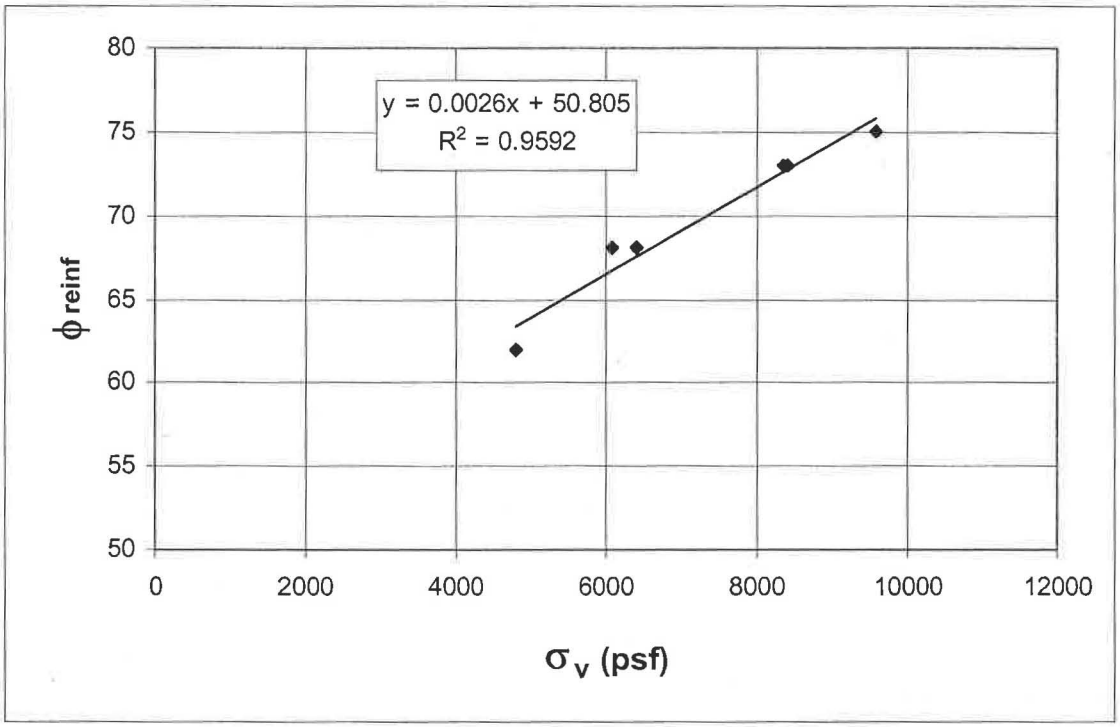


**Figure 7.8** Reinforced Friction Angle and Vertical Stresses on the Sample

### 7.2.4 Reinforced cohesion

The previous section showed that the reinforced friction angle increased as the reinforcement strength increased when the cohesion was held constant at 0.6 ksf (Figure 7.7). To check the effect of increased reinforcement strength on the cohesion value, the angle of friction was held constant at 40° and parallel failure lines were drawn (Figure 7.9).

The Mohr circles of the reinforced samples were again plotted as shown in Figure 7.9. Lines oriented 40° from the horizontal (40° is the backfill friction angle from the direct shear test) and tangent to the circles were drawn (Figure 7.9). The value the intercept the lines make with the vertical axis, $\tau$, were then determined and considered as the reinforced cohesion, $c_{reinf}$ (Figure 7.9). The reinforced cohesion increased as the tensile strength of the reinforcement increased (Figure 7.9 and Table 7.16).

The reinforced cohesion of the sample, $c_{reinf}$, reinforced with TG500 spaced 12 inches apart (TG500-12 in Table 7.16) was 0.63 ksf which was almost equal to the backfill cohesion, c = 0.60 ksf. The sample reinforced with TG500 at 12 inches spacing failed at a low compressive stress. The sample reached peak strength of about 2.7 ksf at 1.5% strain (Figure 5.1) then dropped sharply to less than half its peak. Inspection of the reinforcement after loading showed no rupture in any of the layers indicating that the reinforcement may not have been mobilized to contribute any strength to the sample. The almost equal values of the reinforced cohesion ($c_{reinf}$ = 0.63 ksf) and the backfill cohesion (c = 0.60 ksf) for the sample reinforced with TG500 at 12 inches spacing, was another indication that the reinforcement was not effective and the reinforcement tensile strength was barely mobilized during loading. The reinforced cohesion, $c_{reinf}$, for the samples with reinforcement spaced 6 inches apart were higher than that of the backfill and ranged from 1.13 ksf to 2.25 ksf (Table 7.16).

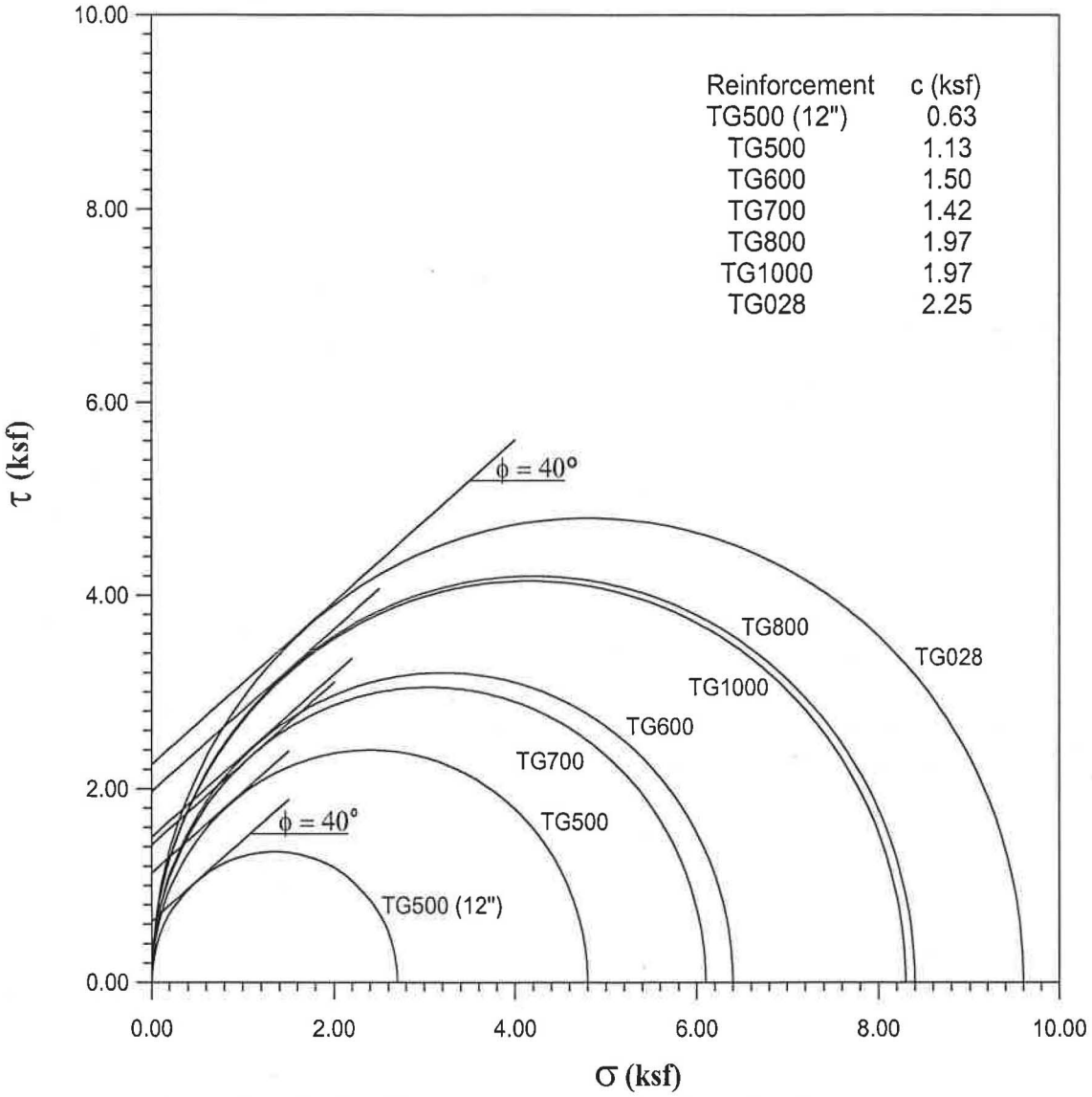


**Figure 7.9** Mohr Circles and $c_{reinf}$ for Reinforced Soil Samples

### 7.2.5 Lateral stress coefficient

The maximum tensile forces in the reinforcement calculated using the proposed equation, $T_{max\ AU}$, were divided by the corresponding sample peak normal stresses, $\sigma_v$. The ratio $T_{max\ AU}/\sigma_v$ can be likened to the lateral stress coefficient and was called $K_{reinf}$. The $K_{reinf}$ value from the $T_{max\ AU}/\sigma_v$ ratio was about 0.050 for all the reinforcement types (Table 7.16).

The $K_{reinf}$ value can also be backcalculated from the proposed equation. The $T_{max\ AU}$ equation is given as:

$$T_{max\ AU} = \sigma_v (K_o - K_a) S_v (SDF)$$

Dividing $T_{max\ AU}$ by $\sigma_v$, the value of $K_{reinf}$ can be backcalculated as:

$$K_{reinf} = \frac{T_{max\ AU}}{\sigma_v} = (K_o - K_a) S_v (SDF)$$

The SDF as well as $K_o$ and $K_a$ are dimensionless. The vertical spacing has units of length (ft). Therefore, $K_{reinf}$ has also units of length (ft). The $(K_o - K_a)$ value is 0.0932 for a backfill friction angle of 40°, $S_v$ is 0.5 ft, and the SDF for maximum tensile stress in the reinforcement is 1.0 at

z/H = 0.5. Using these values would give a backcalculated $K_{reinf}$ value of 0.047 ft, which is close to the calculated value of about 0.05 ft from the $T_{max\ AU}/\sigma_v$ ratio.

A $K_{reinf}$ value of 0.05 ft, therefore, can be used to give a quick estimate of the maximum tensile force in the reinforcement that can be expected given the applied normal load, provided the backfill friction angle is 40° and the reinforcements are spaced 6 inches apart.

**Table 7.16** Reinforced friction angle and lateral stress coefficient.

| Reinforcement | $\phi_{reinf}$ (degrees) | $c_{reinf}$ (ksf) | $T_{max\ AU}$ (lb/ft) | $\sigma_v$ (psf) | $K_{reinf}$ (ft) |
|---|---|---|---|---|---|
| TG500-12 | 42.5 | 0.63 | | | |
| TG500 | 62 | 1.13 | 245.99 | 4800 | 0.051 |
| TG600 | 68 | 1.50 | 320.07 | 6390 | 0.050 |
| TG700 | 68 | 1.42 | 305.16 | 6070 | 0.050 |
| TG800 | 73 | 1.97 | 413.72 | 8400 | 0.049 |
| TG1000 | 73 | 1.97 | 411.39 | 8350 | 0.049 |
| TG028 | 75 | 2.25 | 468.23 | 9570 | 0.049 |

### 7.2.6 Design example

Consider a typical single-span, short (about 50 ft) concrete bridge, weighing about 300 kips, with two-12 ft lanes. Assume two 75-kip trucks on one end of the bridge near the abutment. The load bearing on a 5 ft x 24 ft bridge seat would be about 2.5 ksf or 2500 psf. If the bridge seat were 0.5 ft thick, the dead load from bridge seat would add 75 psf.

The concrete bridge is seating on a reinforced abutment that is 30 ft high. The abutment is composed of a granular backfill with a unit weight of 120 pcf and a friction angle of 40o. The abutment is reinforced with geotextiles spaced 6 inches apart.

The maximum tensile force in the reinforcement of the bridge abutment would be at z/H = 0.85 because the SDF is equal to 1.0 at this point and is decreasing at z/H greater than this (Figure 7.2). The total vertical stress at this depth (z = 25.5) would be calculated as:

$$\sigma_v = \gamma z + q_{DL} + q_{LL}$$

$$\sigma_v = [(120)(25.5)] + 75 + 2500$$

$$\sigma_v = 5635\,\text{psf}$$

The maximum vertical stress would be at the bottom of the wall equal to 6175 psf. This vertical stress is larger than the 3969 psf applied stress on the FHWA abutment. This vertical stress is about 140% of the FHWA abutment applied stress.

Given a backfill friction angle of 40o, the at-rest, Ko, and active, Ka, lateral earth pressure coefficients can be calculated as:

$$K_o = \frac{1-\sin\phi}{1+\sin\phi}\left(1+\frac{2}{3}\sin\phi\right)$$

$$K_o = \frac{1-\sin 40^\circ}{1+\sin 40^\circ}\left(1+\frac{2}{3}\sin 40^\circ\right)$$

$$K_o = 0.3106$$

$$K_a = \tan^2(45-\phi/2)$$

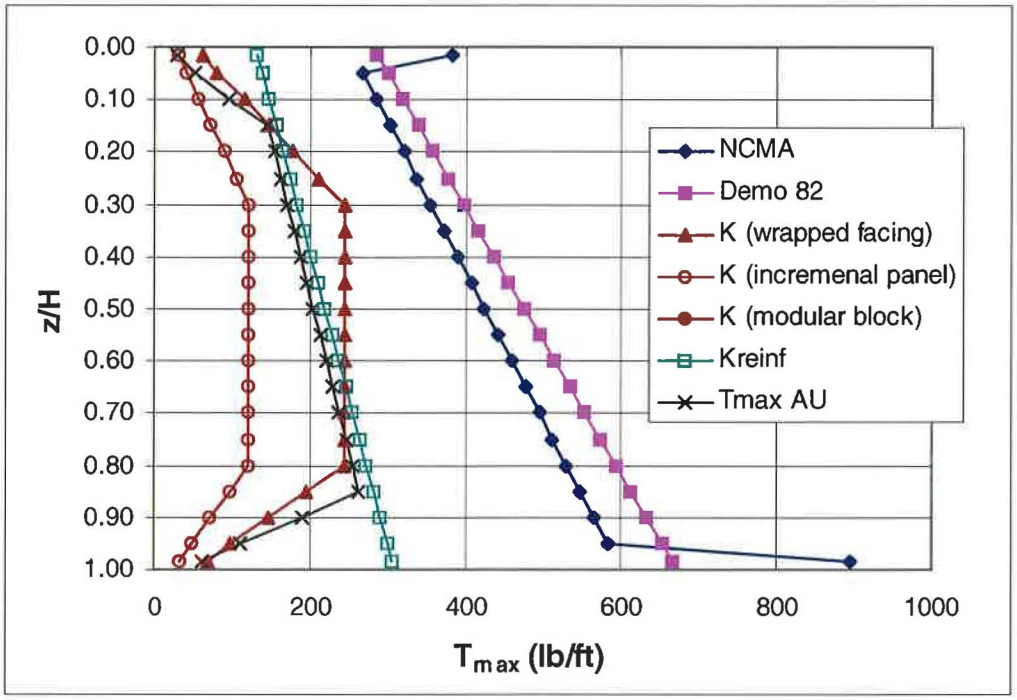


**Figure 7.10** $T_{max}$ values from different methods for the design example

**Table 7.17** Tensile stress values calculated for the design example (lb/ft)

| z/H | $T_{max}$ AU | $T_{max}$ NCMA | $T_{max}$ DEMO 82 | $T_{max}$ K STIFFNESS ($\Phi_{fs}$ = 1.0) | $T_{max}$ K STIFFNESS ($\Phi_{fs}$ = 0.5) | $T_{max}$ K STIFFNESS ($\Phi_{fs}$ = 0.35) | $T_{max}$ Kreinf |
|---|---|---|---|---|---|---|---|
| 0.02 | 27.01 | 381.82 | 286.48 | 60.85 | 30.43 | 21.30 | 121.75 |
| 0.10 | 95.72 | 285.15 | 319.10 | 114.40 | 57.20 | 40.04 | 146.75 |
| 0.15 | 145.13 | 302.64 | 338.67 | 146.04 | 73.02 | 51.12 | 155.75 |
| 0.20 | 153.51 | 320.12 | 358.24 | 177.69 | 88.84 | 62.19 | 164.75 |
| 0.25 | 161.90 | 337.61 | 377.81 | 211.76 | 105.88 | 74.12 | 173.75 |
| 0.30 | 170.29 | 355.10 | 397.38 | 243.41 | 121.70 | 85.19 | 182.75 |
| 0.35 | 178.67 | 372.59 | 416.95 | 243.41 | 121.70 | 85.19 | 191.75 |
| 0.40 | 187.06 | 390.07 | 436.52 | 243.41 | 121.70 | 85.19 | 200.75 |
| 0.45 | 195.44 | 407.56 | 456.09 | 243.41 | 121.70 | 85.19 | 209.75 |
| 0.50 | 203.83 | 425.05 | 475.66 | 243.41 | 121.70 | 85.19 | 218.75 |
| 0.55 | 212.22 | 442.54 | 495.23 | 243.41 | 121.70 | 85.19 | 227.75 |
| 0.60 | 220.60 | 460.02 | 514.80 | 243.41 | 121.70 | 85.19 | 236.75 |
| 0.65 | 228.99 | 477.51 | 534.37 | 243.41 | 121.70 | 85.19 | 245.75 |
| 0.70 | 237.38 | 495.00 | 553.94 | 243.41 | 121.70 | 85.19 | 254.75 |
| 0.75 | 245.76 | 512.49 | 573.51 | 243.41 | 121.70 | 85.19 | 263.75 |
| 0.80 | 254.15 | 529.98 | 593.08 | 243.41 | 121.70 | 85.19 | 272.75 |
| 0.85 | 262.53 | 547.46 | 612.65 | 194.72 | 97.36 | 68.15 | 281.75 |
| 0.90 | 189.64 | 564.95 | 632.22 | 146.04 | 73.02 | 51.12 | 290.75 |
| 0.98 | 62.68 | 893.33 | 664.83 | 68.15 | 34.08 | 23.82 | 305.75 |

| z/H | $\frac{T_{max\ AU}}{T_{max\ DEMO\ 82}}$ | $\frac{T_{max\ AU}}{T_{max\ NCMA}}$ | $\frac{T_{max\ AU}}{T_{max\ Kreinf}}$ |
|---|---|---|---|
| 0.02 | 0.094 | 0.071 | 0.205 |
| 0.10 | 0.300 | 0.336 | 0.652 |
| 0.15 | 0.429 | 0.480 | 0.932 |
| 0.20 | 0.429 | 0.480 | 0.932 |
| 0.25 | 0.429 | 0.480 | 0.932 |
| 0.30 | 0.429 | 0.480 | 0.932 |
| 0.35 | 0.429 | 0.480 | 0.932 |
| 0.40 | 0.429 | 0.480 | 0.932 |
| 0.45 | 0.429 | 0.480 | 0.932 |
| 0.50 | 0.429 | 0.480 | 0.932 |
| 0.55 | 0.429 | 0.480 | 0.932 |
| 0.60 | 0.420 | 0.480 | 0.932 |
| 0.65 | 0.429 | 0.480 | 0.932 |
| 0.70 | 0.429 | 0.480 | 0.932 |
| 0.75 | 0.429 | 0.480 | 0.932 |
| 0.80 | 0.429 | 0.480 | 0.932 |
| 0.85 | 0.429 | 0.480 | 0.932 |
| 0.90 | 0.300 | 0.336 | 0.652 |
| 0.98 | 0.094 | 0.070 | 0.205 |

**Table 7.19** Ratio of $T_{max\ AU}$ with $T_{max\ K\ STIFFNESS}$ for the design example

| z/H | $\frac{T_{max\ AU}}{T_{max\ K\ STIFFNESS}}$ ($\Phi_{fs} = 1.0$) | $\frac{T_{max\ AU}}{T_{max\ K\ STIFFNESS}}$ ($\Phi_{fs} = 0.5$) | $\frac{T_{max\ AU}}{T_{max\ K\ STIFFNESS}}$ ($\Phi_{fs} = 0.35$) |
|---|---|---|---|
| 0.02 | 0.444 | 0.888 | 1.268 |
| 0.10 | 0.837 | 1.673 | 2.391 |
| 0.15 | 0.994 | 1.987 | 2.839 |
| 0.20 | 0.864 | 1.728 | 2.468 |
| 0.25 | 0.765 | 1.529 | 2.184 |
| 0.30 | 0.700 | 1.399 | 1.999 |
| 0.35 | 0.734 | 1.468 | 2.097 |
| 0.40 | 0.769 | 1.537 | 2.196 |
| 0.45 | 0.803 | 1.606 | 2.294 |
| 0.50 | 0.837 | 1.675 | 2.393 |
| 0.55 | 0.872 | 1.744 | 2.491 |
| 0.60 | 0.906 | 1.813 | 2.589 |
| 0.65 | 0.941 | 1.882 | 2.688 |
| 0.70 | 0.975 | 1.950 | 2.786 |
| 0.75 | 1.010 | 2.019 | 2.885 |
| 0.80 | 1.044 | 2.088 | 2.983 |
| 0.85 | 1.348 | 2.696 | 3.852 |
| 0.90 | 1.299 | 2.597 | 3.710 |
| 0.98 | 0.920 | 1.839 | 2.628 |

The tensile stress in the reinforcement is affected by the soil type, depth of embedment, surcharge, and vertical spacing. The allowable tensile strength, $T_a$, of the geosynthetic reinforcement can be calculated as (Elias and Christopher, 1996):

$$T_a = \frac{T_{ult}}{RF_D \; RF_{ID} \; RF_{CR} \; FS}$$

where $T_{ult}$ is the ultimate or yield tensile strength from wide width tensile strength tests; FS is the overall factor of safety or load reduction factor to account for uncertainties in the geometry of the structure, fill properties, reinforcement properties, and externally applied loads; and $RF_D$, $RF_{ID}$, $RF_{CR}$ are the durability, installation damage, and creep reduction factors. Typical value for FS is 1.5. Typical ranges of reduction factors are 1.1 to 2.0 for durability, 1.05 to 3.0 for installation damage, and 4.0 to 5.0 for creep for polypropylene geosynthetics.

Taking the reduction factors as equal to 1.1 for durability, 1.05 for installation damage, and 4.0 for creep and taking FS equal to 1.5, the required ultimate tensile strength of the reinforcement was calculated as equal to about 7 times the allowable tensile strength:

$$T_a = \frac{T_{ult}}{1.1 * 1.05 * 4.0 * 1.5}$$

$$T_a = \frac{T_{ult}}{6.93}$$

$$T_{ult} = 7\,T_a$$

The applied force in the reinforcement during loading should not exceed the allowable tensile strength. Setting the calculated tensile force in the reinforcement, Tmax AU equal to the allowable tensile strength, Ta, the required ultimate tensile strength, Tult, of the reinforcement was calculated as:

$$T_{ult} = 7\,T_{max\,AU}$$

The calculated ultimate tensile strength requirements of the reinforcements for the different methods are given in Table 7.20.

**Table 7.20** Ultimate tensile strength requirements for the design example (lb/ft)

| z/H | $T_{ult}$ AU | $T_{ult}$ NCMA | $T_{ult}$ DEMO 82 | $T_{ult}$ K STIFFNESS ($\Phi_{fs}$ = 1.0) | $T_{ult}$ K STIFFNESS ($\Phi_{fs}$ = 0.5) | $T_{ult}$ K STIFFNESS ($\Phi_{fs}$=0.35) | $T_{ult\ Kreinf}$ |
|---|---|---|---|---|---|---|---|
| 0.02 | 189.06 | 2672.71 | 2005.37 | 425.96 | 212.98 | 149.09 | 922.25 |
| 0.10 | 670.03 | 1996.03 | 2233.68 | 800.80 | 400.40 | 280.28 | 1027.25 |
| 0.15 | 1015.89 | 2118.45 | 2370.67 | 1022.30 | 511.15 | 357.81 | 1090.25 |
| 0.20 | 1074.59 | 2240.86 | 2507.66 | 1243.80 | 621.90 | 435.33 | 1153.25 |
| 0.25 | 1133.30 | 2363.28 | 2644.65 | 1482.34 | 741.17 | 518.82 | 1216.25 |
| 0.30 | 1192.00 | 2485.69 | 2781.64 | 1703.84 | 851.92 | 596.34 | 1279.25 |
| 0.35 | 1250.70 | 2608.10 | 2918.63 | 1703.84 | 851.92 | 596.34 | 1342.25 |
| 0.40 | 1309.41 | 2730.52 | 3055.62 | 1703.84 | 851.92 | 596.34 | 1405.25 |
| 0.45 | 1368.11 | 2852.93 | 3192.60 | 1703.84 | 851.92 | 596.34 | 1468.25 |
| 0.50 | 1426.81 | 2975.35 | 3329.59 | 1703.84 | 851.92 | 596.34 | 1531.25 |
| 0.55 | 1485.52 | 3097.76 | 3466.58 | 1703.84 | 851.92 | 596.34 | 1594.25 |
| 0.60 | 1544.22 | 3220.17 | 3603.57 | 1703.84 | 851.92 | 596.34 | 1657.25 |
| 0.65 | 1602.92 | 3342.59 | 3740.56 | 1703.84 | 851.92 | 596.34 | 1720.25 |
| 0.70 | 1661.63 | 3465.00 | 3877.55 | 1703.84 | 851.92 | 596.34 | 1783.25 |
| 0.75 | 1720.33 | 3587.42 | 4014.54 | 1703.84 | 851.92 | 596.34 | 1846.25 |
| 0.80 | 1779.03 | 3709.83 | 4151.53 | 1703.84 | 851.92 | 596.34 | 1909.25 |
| 0.85 | 1837.74 | 3832.25 | 4288.52 | 1363.07 | 681.53 | 477.07 | 1972.25 |
| 0.90 | 1327.51 | 3954.66 | 4425.51 | 1022.30 | 511.15 | 357.81 | 2035.25 |
| 0.98 | 438.74 | 6253.33 | 4653.82 | 477.07 | 238.54 | 166.98 | 2140.25 |

### 7.2.7 Analysis: Reinforcement tensile strength requirement

The $T_{max\ AU}$ values were more conservative (i.e. larger) compared to that calculated using the K stiffness method assuming a segmental concrete block facing ($\Phi_{fs}$ = 0.35) or an incremental panel facing ($\Phi_{fs}$ = 0.5). The two methods were almost equal for a wrapped wall facing ($\Phi_{fs}$ = 1.0). However, the $T_{max\ AU}$ values were only about half of that calculated using the NCMA and Demo 82 Methods. This means savings can be generated by using reinforcements with half the tensile strength requirements calculated using the NCMA and Demo 82 methods.

The trapezoidal distribution of the forces in the proposed equation demonstrated that the most critical reinforcements were the middle layers. The tensile forces calculated using the NCMA method has a wedge distribution at z/H = 0.2 to 0.8 with larger values at the top (z/H = 0.1) and bottom (z/H = 0.9) layers. The tensile forces calculated using the Demo 82 method also has a wedge-shaped distribution with forces increasing with depth. The change in the shape of the stress distribution to a trapezoidal distribution for $T_{max\ PROPOSED}$, showed that the high strength reinforcement requirements normally required by the NCMA and Demo 82 methods at the top (z/H < 0.15) and bottom (z/H > 0.85) of a wall/abutment to resist large stresses, could be reduced.

## VIII. CONCLUSIONS

Large cylindrical reinforced soil samples were axisymmetrically loaded in compression. The backfill was poorly graded sand reinforced with spunbonded, needlepunched, nonwoven geotextiles. A load cell attached to the 300 kip hydraulic ram, three transducers on top of the steel loading plate to measure vertical displacements, and linear potentiometers to measure lateral displacements were monitored by an automated data acquisition system during testing.

1. The reinforcement spacing of 12 inches was too far apart for the reinforcement to be effective, based on one sample tested in the laboratory.
2. The friction angle of the sample reinforced with TG500 spaced 12 inches apart, $\phi_{reinf}$ = 42.5°, was almost equal to the backfill friction angle, $\phi$ = 40° when the cohesion value was fixed at 0.60 ksf. When the friction angle was fixed at 40°, the reinforced cohesion, $c_{reinf}$ = 0.63 ksf, was almost equal to the backfill cohesion value, c = 0.60 ksf. These indicate that the reinforcement strengths were not mobilized and contributed little or none at all to the strength of the reinforced sample.
3. Peak strengths of 4.8 ksf to 9.6 ksf at 3% to 8% vertical strain can be obtained from reinforced samples with reinforcements at 6-inch spacing (Figure 5.1). This suggests that a pileless bridge abutment, moderately reinforced with at least a 50 lb/in wide-width tensile strength geotextile spaced at 6 inches, can support a modest 50 ft single span bridge with an applied stress of about 2.5 ksf.
4. Reinforced soils have larger strains to failure and failure is not immediate.
5. The use of a stronger geotextile produced a stiffer, i.e. higher modulus, reinforced soil.
6. Location of tears in the reinforcements verified that maximum lateral strains occurred at the middle of the sample (Figure 4.14) and that the middle layers (z/H = 0.4) of reinforcement were the first to be mobilized.
7. The strains in the reinforcement when plotted against z/H had a trapezoidal distribution. A new factor called the strain distribution factor (SDF) was developed based on the normalized strains of the reinforcement during loading. The new SDF was used in the proposed equation to calculate the maximum tensile force in the reinforcement. The SDF enabled the proposed equation to closely mimic the distribution of stress of the reinforcement during loading wherein strains were maximum in the middle layers and reduced at the ends. The tensile stresses were maximum at z/H of 0.15 to 0.85 and decreasing above and below that zone.
8. A lateral earth pressure coefficient, K, was calculated as $(K_o - K_a)$ where $K_o$ and $K_a$ are given as:

$$K_o = \frac{1 - \sin\phi}{1 + \sin\phi}\left(1 + \frac{2}{3}\sin\phi\right)$$

$$K_a = \tan^2(45 - \phi/2)$$

The K value was derived empirically by comparing the maximum tensile force in the reinforcement, $T_{max\ AU}$, to the tension force, T, estimated from the strain. The K value equal to $(K_o - K_a)$, among various tested K values such as $K_o = 1 - \sin\phi$, gave a $T_{max\ AU}$ value that is greater than and closer to the estimated tensile force in the reinforcement, T.

9. The ratio of the geotextile ultimate tensile strength from wide-width tensile strength tests (ASTM D4595), $T_{ult}$, with the maximum tensile force in the reinforcement, $T_{max\ AU}$, should be greater than or equal to 3.50 (Table 8.14) to ensure that no layer of reinforcement will rupture.
10. The friction angles of the reinforced sample, $\phi_{reinf}$, were greater than the backfill friction angle, $\phi$, when the cohesion value was held constant for the samples with reinforcements

spaced 6 inches apart (Figure 8.7). In the same way, the cohesion values of the reinforced sample, $c_{reinf}$, were greater than the backfill cohesion, c, when the friction angle was held constant (Figure 8.9). These indicate that for samples reinforced at 6-in spacing, the reinforcement strengths were mobilized and contributed to the strength of the reinforced sample.

11. The lateral stress coefficient, $K_{reinf}$, derived from the ratio of $T_{max\ AU}$ with the applied vertical stress, $\sigma_v$, was equal to about 0.05 for all reinforcement types at 6-inch spacing. The $K_{reinf}$ = 0.05 value can be multiplied by the applied vertical stress to give a quick estimate of the maximum tensile force developed in the reinforcement provided that the backfill friction angle is 40° and the reinforcements are spaced 6 inches apart.

## IX. RECOMMENDATIONS FOR ABUTMENT DESIGN

Unconfined compression tests on large geotextile reinforced samples led to the development of the proposed equation, shown below, to calculate the tensile strength of the reinforcement.

Spunbonded, needlepunched, nonwoven geotextiles were used to reinforce a poorly graded sand backfill. The reinforced soil samples were axisymmetrically loaded in compression. Instrumentation consisted of a load cell attached to the 300 kip hydraulic ram, three transducers on top of the steel loading plate to measure vertical displacements, and linear potentiometers to measure lateral displacements. Data were monitored and collected by an automated data acquisition system during testing.

The tensile stresses developed in the geotextile were calculated by determining the strains in the reinforcements and multiplying it with the corresponding modulus obtained from the wide-width tensile strength tests.

The proposed equation, given below, was developed by using the factors affecting the tensile strength of the reinforcement: vertical stress, earth pressure coefficient, and the vertical spacing. The vertical stresses due to the weight of the backfill soil on top of the reinforcement were modified for depths greater than mid-height. A unique factor, the strain distribution factor (SDF), derived from the normalized strains in the reinforcement was integrated in the equation.

It is recommended that the tensile force in the reinforcement in a mechanically stabilized earth bridge abutment be calculated as:

$$T_{max\ AU} = [(\gamma z + q_{DL} + q_{LL})\ (K_o - K_a)]\ (S_v)\ (SDF)$$

where $\gamma$ = unit weight of the backfill

$z$ = depth of reinforcement

$q_{DL}$ = applied dead load

$q_{LL}$ = applied live load

$K_o$ = at-rest earth pressure coefficient calculated using Jaky's equation:

$$K_o = \frac{1 - \sin\phi}{1 + \sin\phi}\left(1 + \frac{2}{3}\sin\phi\right)$$

$K_a$ = Rankine's active earth pressure coefficient calculated as:

$$K_a = \tan^2 (45 - \phi/2)$$

$S_v$ = tributary vertical distance taken as the vertical spacing between reinforcements

SDF = the strain distribution factor from the strain distribution curve (Figure 7.2)

The proposed equation for $T_{max}$, while preliminary, bears further investigation, and may lead to a more confident and economical design of pileless bridge abutments.

## BIBLIOGRAPHY


AASHTO LRFD Bridge Design Specifications 2nd ed (1998). American Association of State Highway and Transportation Officials. Washington, D. C.

Abu-Hejleh, N. M, Outcalt, W., Wang, T. and Zornberg, J.G. (2000). Performance of Geosynthetic-Reinforced Walls Supporting the Founders/Meadows Bridge and Approaching Roadway Structures – Report 1: Design, Materials, Construction, Instrumentation and Preliminary Results. Colorado Department of Transportation Report No. CDOT-DTD-R-2000-5. Colorado Department of Transportation, Denver, Colorado.

Abu-Hejleh, N. M., Zornberg, J.G., Elias, V. and Watcharamonthein, J. (2003). Design Assessment of Founders-Meadows GRS Abutment Structure. Proceedings of the Transportation Research Board 82nd Annual Meeting. Washington, D. C.

Abu-Hejleh, N. M., Zornberg, J. G. and Wang, T (2001). Monitored Displacements of a Unique Geosynthetic-Reinforced Walls Supporting Bridge and Approaching Roadway Structures. Proceedings of the Transportation Research Board 80th Annual Meeting. Washington, D. C.

Adams, M. (2000). Reinforced Soil Technology - Making Old Technology New. Geotechnical Fabrics Report Vol. 18 No. 6 pp. 34-37.

Adams, M., Ketchart, K., Ruckman, A., DiMillio, A.F., Wu, J., and Satyanarayana, R. (1999). Reinforced Soil for Bridge Support Applications on Low-Volume Roads. Transportation Research Record No. 1652, Washington, D.C., pp. 150-160.

Allen, T. M. and Bathurst, R. (2001). Application of the Ko-Stiffness Method to Reinforced Soil Wall Limit States Design. Final Research Report to the Washington State Department of Transportation.

Allen, T. M., Christopher, B. R. and Holtz, R. D. (1992). Performance of a 12.6 m High Geotextile Wall in Seattle, Washington. Geosynthetic Reinforced Soil Retaining Walls, J. T. H. Wu (editor), Balkema, Rotterdam, pp. 81-100.

Allen, T. M., Bathurst, R. J., Holtz, R. D., Walters, D. and Lee, W. F. (2003). A New Working Stress Method for Prediction of Reinforcement Loads in Geosynthetic Walls. Canadian Geotechnical Journal, Vol. 40, No 5, pp. 976-994.

Al-Omari, R.R., Nazhat, Y.N., and Dobaissi, H.H. (1995). Effect of Stiffness and Amount of Reinforcement on Strength of Sand. Journal of Engineering Geology Vol. 28, pp. 363-367.

Ashmawy, A.K. and Bourdeau, P.L. (1998). Effect of Geotextile Reinforcement on the Stress-Strain and Volumetric Response of Sand. Proceedings of the Sixth International Conference on Geosynthetics, Atlanta, Vol. 2, pp. 1079-1082.

ASTM D1557. Standard Test Methods for Laboratory Compaction Characteristics of Soil Using Modified Effort (56,000 ft-lbf/ft3 (2,700 kN-m/m3)). American Society for Testing and Materials. West Conshohocken, PA, USA.

ASTM D3080. Standard Test Method for Direct Shear Test of Soils Under Consolidated Drained Conditions. American Society for Testing and Materials. West Conshohocken, PA, USA.

ASTM D4595. Standard Test Method for Tensile Properties of Geotextiles by the Wide-Width Strip Method. American Society for Testing and Materials. West Conshohocken, PA, USA.

Athanasopoulos, G.A. (1993). Effect of Particle Size on the Mechanical Behavior of Sand-Geotextile Composites. Geotextiles and Geomembranes Vol. 12 pp. 255-273

Atmatzidis, D.K. and Athanasopoulos, G. A. (1994). Sand-Geotextile friction angle by conventional shear testing. XIII International Conference on Soil Mechanics and Foundation Engineering, pp. 1273-1278.

Barrett, B. and Ruckman, A. (1996). Geosynthetics in Jamaica. Geotechnical Fabrics Report, Vol. 14, No. 5, pp. 28-31.

Bathurst, R. J. (1993). Investigation of Footing Restraint on Stability of Large-Scale Reinforced Soil Wall Tests. Forty-Sixth Annual Canadian Geotechnical Conference. Saskatuan, Saskatuan, pp. 389-398.

Bathurst, R. J. and Benjamin D. J. (1990). Failure of a Geogrid-Reinforced Soil Wall. Transportation Research Record 1288. Washington, D. C., pp. 109-116.

Bathurst, R. J., Allen, T. M. and Walters, D. (2003). Reinforcement Loads in Geosynthetic Walls and the Case for a New Working Stress Design Method. The Mercer Lecture. Fifty-Sixth Canadian Geotechnical Conference and Fourth Joint IAH-CNC/CGS Conference. Winnipeg, Manitoba, Canada.

Bathurst, R. J., Jarrett, P. M. and Lescoutre, S. R. (1988). An Instrumented Wrap-Around Geogrid Reinforced Soil Wall. Third Canadian Symposium on Geosynthetics, Kitchener, Ontario, pp. 71-78.

Bathurst, R. J., Wawrychuk, W. F. and Jarrett, P.M. (1987). Laboratory Investigation of Two Large-Scale Geogrid Reinforced Soil Walls. The Application of Polymeric Reinforcement in Soil Retaining Structures. NATO Advanced Study Institutes Series, Kluwer Academic Publishers, pp 75-125.

Berg, R. R., Bonaparte, R., Anderson, R. P. and Chouery, V. E. (1986). Design, Construction, and Performance of Two Geogrid Reinforced Soil Retaining Walls. Proceedings of the Third International Conference on Geotextiles. Vienna, pp. 401-406.

Bergado, D.T., Werner, G., Tien, M.H. and Zou, X.H. (1995). Interaction Between Geotextiles and Silty-Sand by Large Direct Shear and Triaxial Tests. Geosynthetics Conference Vol. 3 pp. 1097-1109.

Bonaparte, R. and Schmertmann, G. R. (1987). Reinforcement Extensibility in Reinforced Soil Wall Design. The Application of Polymeric Reinforcement in Soil Retaining Structures. NATO Advanced Study Institutes Series, Kluwer Academic Publishers, pp. 409-457.

Bowles, J.E. (1988). Foundation Analysis and Design, 4th ed. McGraw-Hill Book Company.

Boyd, M. S. (1988). Reinforced Earth Bridge Abutments. International Geotechnical Symposium on Theory and Practice of Earth Reinforcement. Fukuoka, Japan, pp. 499-503.

Bright, D. G., Collin, J. G. and Berg, R. R. (1994). Durability of Geosynthetic Soil Reinforcement Elements in Tanque Verde Retaining Wall Structures. Transportation Research Record 1439. Washington, D. C., pp. 46-54.

Broms, B.B. (1977). Triaxial Tests with Fabric-Reinforced Soil. Proc. of the Intl Conf on the use of fabric in Geotechnics Vol. 3. Ecole Nationale des Ponts et Chaussees, Paris, pp. 129-134.

Chandrasekaran, B., Broms, B. and Wong, K. S. (1989). Strength of Fabric Reinforced Sand under Axisymmetric Loading. Geotextiles and Geomembranes, Vol. 8, pp. 293-310.

Christopher, B. R. (1993). Deformation Response and Wall Stiffness in Relation to Reinforced Soil Wall Design. PhD Dissertation, Purdue University. 352 pages.

Devin, S.C., Keller, G.R., Barrett, R.K. (2001). Geosynthetic Reinforced Soil (GRS) Bridge Abutments fill the Gap at Mammoth Lakes, California. Proc. 36th Annual Engineering Geology and Geotechnical Engineering Symposium, March 28-31, 2001, University of Nevada, Las Vegas, Las Vegas, NV.

Elias, V. and Christopher, B.R. (1996). Mechanically Stabilized Earth Walls and Reinforced Soil Slopes – Design and Construction Guidelines. FHWA Demonstration Project 82. Federal Highway Administration, McLean, VA, USA.

Futaki, M., Suzuki, H., and Yamato, S. (1990). Super Large Triaxial Tests on Reinforced Sand with High Strength Geogrid. Proceedings of the 4th International Conference on Geotextiles, Geomembranes and Related Products Vol. 2 pp. 759-764.

Gray, D.H. and Al-Refeai, T. (1986). Behavior of Fabric vs. Fiber-Reinforced Sand. Journal of Geotechnical Engineering, ASCE, Vol. 112, No. 8, pp. 804-820.

Gray, D.H., Athanasopoulos, G.A., and Ohashi, H. (1982). Internal/External Fabric Reinforcement of Sand. Proceedings of the 2nd International Conference on Geotextiles. Vol. 3, pp. 805-809.

Haeri, S.M., Noorzad, R., and Oskoorouchi, A.M. (2000). Effect of Geotextile Reinforcement on the Mechanical Behavior of Sand. Geotextiles and Geomembranes, Vol. 18, pp. 385-402.

Jones, C.J.F.P. (1996). Earth Reinforcement and Soil Structures. Thomas Telford. ASCE Press.

Juran, I., Guermazi, A., Chen, C.L. and Ider, M.H. (1988). Modelling and Simulation of Load Transfer in Reinforced Soils: Part 1. International Journal for Numerical and Analytical Methods in Geomechanics Vol. 12 pp. 141-155.

Kasugai, A. and Tateyama, M. (1992). Application of Geosynthetic-Reinforced Soil for Bridge Abutments. . Earth Reinforcement Practice. Ochiai, Hayashi and Otani (eds). Balkema, Rotterdam, pp. 363-368.

Ketchart, K. and Wu, J. T. H. (1997). Loading Test of GRS Bridge Pier and Abutment in Denver, Colorado. Colorado Department of Transportation Report No. CDOT-DTD-97-10. Colorado Department of Transportation, Denver, Colorado.

Ketchart, K. and Wu, J. T. H. (2001). Performance Test for Geosynthetic-Reinforced Soil including Effects of Preloading. Federal Highway Administration Report No. FHWA-RD-01-018. Federal Highway Administration, McLean, VA, USA.

Koerner, R.M. (1998). Designing with Geosynthetics, 4th ed., Prentice-Hall, Inc.

Krishnaswamy, N.R. and Isaac, N.T. (1995). Liquefaction Analysis of Saturated Reinforced Granular Soils. Journal of Geotechnical Engg ASCE Vol. 121 No. 9 pp 645-651.

Kumada, T., Otani, Y. and Matsui, T. (1992). Practice and Design of Reinforced Earth Bridge Abutments on Soft Ground. Earth Reinforcement Practice. Ochiai, Hayashi and Otani (eds). Balkema, Rotterdam, pp. 373-378.

Lee, W. F. (2000). Internal Stability Analyses of Geosynthetic Reinforced Retaining Walls. PhD Dissertation, University of Washington, Washington State, USA.

Long, N.T., Legeay, G., and Madani, C. (1983). Soil-Reinforcement Friction in a Triaxial Test. Proceedings of the 8th European Conference on Soil Mechanics and Foundation Engineering, Vol. 1, pp. 381-384.

Matichard, Y., Balzer, E., Delmas, P., Fargeix, D., Thamm, B., and Sere, A. (1992). Behaviour of a Geotextile Reinforced Soil Abutment – Full Scale and Centrifuge Models. Earth Reinforcement Practice. Ochiai, Hayashi and Otani (eds). Balkema, Rotterdam, pp. 379-384.

National Concrete Masonry Association (1996). Design Manual for Segmental Retaining Walls, 2nd ed. Collin, J.G. – editor.

Ng, H. Y. and Mak, C. H. (1988). A 14 Metre High Reinforced Soil Embankment as the Abutment of a Steel Bridge in Tuen Mun, Hong Kong. International Geotechnical Symposium on Theory and Practice of Earth Reinforcement. Japan, pp. 449-454.

Powell, W., Keller, G.R. and Brunette, B. (1999). Applications for Geosynthetics on Forest Service Low Volume Roads. Transportation Research Record No. 1652. Washington, D. C., pp. 113-120.

Rekenthaler, D. (1997). Geosynthetic Reinforced Soil Piers: A Bridge from the Past to the Present. http://www.tfhrc.gov/pubrds/winter97/p97wi43.htm. Public Roads On-Line, Vol. 60, No. 3. Accessed May 2003.

SI Geosolutions. http://www.fixsoil.com. Accessed February 2004.

Turner-Fairbank Highway Research Center Geotechnical (GT) Research Team http://www.tfhrc.gov/structur/gtr/main.htm. Accessed May 2003.

Vidal, H. (1969). The Principle of Reinforced Earth. Highway Research Record 282, Highway Research Board, National Research Council. Washington, D.C. pp. 1-24.

Vulova, C. and Leshchinsky, D. (2003). Effect of Geosynthetic Reinforcement Spacing on the Performance of Mechanically Stabilized Earth Walls. Publication No. FHWA-RD-03-048. Federal Highway Administration, McLean, VA, USA.

Wu, J.T.H., Ketchart, K. and Adams, M. (2001). GRS Bridge Piers and Abutments. FHWA Report No. FHWA-RD-00-038. Federal Highway Administration, McLean, VA, USA.

Yang, Z. (1972). Strength and Deformation Characteristics of Reinforced Sand. PhD Dissertation, University of California at Los Angeles.

Yenter Companies, Inc. Fortress Abutments and Piers. http://www.yenter.com/abutments.htm. Accessed May 2003.

Zornberg, J.G., Abu-Hejleh, N. and Wang, T. (2001) Geosynthetic-reinforced Soil Bridge Abutments – Measuring the Performance of Geosynthetic Reinforcement in a Colorado Bridge Structure. Geotechnical Fabrics Report Vol. 19 No. pp. 52-55.